ADP-12-16/T783

Threshold Corrections in the Exceptional Supersymmetric Standard Model

Peter Athron*, Dominik Stöckinger†, Alexander Voigt†

* *ARC Centre of Excellence for Particle Physics at the Terascale, School of Chemistry and Physics, University of Adelaide, Adelaide, SA 5005, Australia*

† *Institut für Kern und Teilchenphysik, TU Dresden, Dresden, D-01062, Germany.*

Abstract

We calculate threshold corrections to the running gauge and Yukawa couplings in the Exceptional Supersymmetric Standard Model (E_6SSM) and analyse the more precise and reliable mass spectra in a constrained model (CE_6SSM). Full expressions for the corrections are provided and the implementation into a spectrum generator is described. We find a dramatic reduction in the matching scale dependency of the masses of many states and observe a significant adjustment of the correlation of low-scale physical masses and high-scale parameters. Still, in substantial regions of parameter space the mass of the lightest Higgs is compatible with the new boson discovered at the LHC and the model satisfies limits from collider searches for squark, gluinos and Z' bosons. We study the implications for gauge coupling unification from a new dependency of the spectrum on so-called survival Higgs fields which cannot be addressed without the inclusion of the threshold corrections.

Contents

1 Introduction

Supersymmetric (SUSY) extensions of the Standard Model (SM) with TeV-scale SUSY breaking provide very attractive models for new physics which could be discovered at the Large Hadron Collider (LHC). Such models can solve the hierarchy problem of the SM due to the cancellation of quadratic divergences, enable embedding into Grand Unified Theories (GUTs), and thereby provide an explanation of the $U(1)_Y$ rational charges, postulated *ad hoc* in the SM. These fundamental motivations do not imply any minimality condition on the particle content or gauge structure.

Here we consider the Exceptional Supersymmetric Standard Model[1] (E_6SSM) [2, 3], which is a non-minimal SUSY extension of the SM with an extra $U(1)_N$ gauge symmetry and new exotic matter at the TeV scale. A new Higgs singlet together with an extra $U(1)$ gauge symmetry solve the well-known μ-problem [4] of the Minimal Supersymmetric Standard Model (MSSM) without introducing the tadpole or domain wall problems of the Next-to-MSSM[2] [6]. These features also allow the lightest Higgs boson to be substantially heavier than in the MSSM or NMSSM already at tree-level, through new $U(1)_N$ D-term contributions and an additional F-term contribution from the superpotential coupling between the singlet and doublet Higgs bosons, which can be substantially larger than the parallel NMSSM term due to different perturbative limits on the coupling [3].

The model is inspired and motivated by E_6 GUTs, as the extra $U(1)$ appears from the breakdown of E_6 and the exotic new matter comes from complete E_6 multiplets surviving to low energies, ensuring the cancellation of gauge anomalies. The extra $U(1)$ gauge group of the E_6SSM is uniquely chosen such that right-handed neutrinos are neutral, allowing large Majorana masses and a high-scale see-saw mechanism.

The E_6 symmetry itself can arise from $E_8 \times E_8'$ Heterotic string theory after the breakdown of E_8 [7]. The E_8' then plays the role of a hidden sector interacting with the visible sector only through gravitational interactions and leads to TeV-scale SUSY breaking, generating a set of soft SUSY-breaking parameters.

In recent publications [8, 9] a constrained version (CE_6SSM) was introduced where all the soft SUSY-breaking masses are determined by a universal scalar mass, m_0, gaugino mass $M_{1/2}$ and soft trilinear scalar coupling A. Owing to the unification of matter and Higgs fields in complete GUT multiplets the CE_6SSM is particularly

[1] For a brief review see [1].

[2] Reviews are given in [5].

well motivated. In Refs. [8, 9] the low-energy mass spectra were explored for the first time with benchmark scenarios, representing the phenomenologically distinct possibilities in the model. This work has recently been updated to look at spectra which are consistent with the 125 GeV Higgs signal and recent searches for squarks and gluinos [10]. Other aspects of this model and similar variants have also been discussed in Refs. [11, 12, 13, 14, 15, 16, 17, 18, 19, 20, 21].

The calculations in Refs. [8, 9, 10] neglect important threshold corrections and involve a significant dependence on unphysical threshold scales. This limits the accuracy of phenomenological results and it was stated that the precision for the masses was not better than 10%.

However to facilitate model discrimination from data, and ultimately to reconstruct parameters in the event of a signal, precise predictions of the TeV scale SUSY masses predicted from GUT scale parameters are important. Indeed for the MSSM there are already a number of state of the art spectrum generators publicly available [22, 23, 24, 25, 26] which calculate the spectrum for scenarios, such as the constrained MSSM (CMSSM). Typically these employ two-loop renormalization group equations, full one-loop matching conditions for gauge and Yukawa couplings and one-loop shifts to pole masses and comparisons of their predicted masses suggests an accuracy of about 1% [27].

The present paper is devoted to the calculation of threshold corrections to the running gauge and Yukawa couplings in the Exceptional Supersymmetric Standard Model (E_6SSM), which enable a more precise evaluation of the mass spectrum from high-scale assumptions, and to an extensive study of the phenomenological consequences in the CE_6SSM. As in Refs. [8, 9, 10] we employ two-loop renormalization group equations for the running of the gauge and Yukawa couplings between the weak scale and the GUT scale. As a major improvement, we also compute and take into account the corresponding one-loop threshold corrections arising in the transition from the full CE_6SSM to the SM as a low-energy effective theory. We show that the individual threshold corrections indeed drastically reduce the dependence of our results on the unphysical threshold scale. The resulting, more accurate and reliable mass spectra are discussed. Particular attention is paid to the prediction for the Higgs mass and the gluino mass. We confirm the recent result of Ref. [10] that the lightest Higgs mass can easily be in agreement with recent LHC discovery of a new boson [28, 29]. Finally we use our improved precision to study gauge coupling unification[3] for the CE_6SSM and the impact of the survival Higgs sector, which

[3]Previous studies [30, 31] used trivial matching conditions, equivalent to assuming all new

appears only via threshold corrections.

This paper is structured as follows. In Sec. 2 we briefly outline the E_6SSM model, in Sec. 3 we describe the improved spectrum calculations, give analytical results for the threshold corrections. Sec. 4 describes the application to an improved CE$_6$SSM spectrum generator and explains the full numerical procedure used. In Sec. 5 we illustrate the effect of the thresholds and the improvement in accuracy of our results, and we give an extensive discussion of the resulting model predictions.

2 The E$_6$SSM

The E$_6$SSM is a supersymmetric gauge theory, inspired by E_6 GUTs in which the E_6 is broken at the GUT scale M_X via the Hosotani mechanism [32] down to the low-energy gauge group of the E$_6$SSM,

$$SU(3)_{\rm c} \times SU(2)_{\rm L} \times U(1)_Y \times U(1)_N. \tag{1}$$

Here the $U(1)_N$ is a special case of a $U(1)'$ symmetry arising from E_6 breaking,

$$U(1)' = U(1)_\chi \cos\theta + U(1)_\psi \sin\theta, \tag{2}$$

with $\tan\theta = \sqrt{15}$, where the gauge groups $U(1)_\chi$ and $U(1)_\psi$ are defined by the breaking of $E_6 \to SO(10) \times U(1)_\psi$ and $SO(10) \to SU(5) \times U(1)_\chi$ [33, 34].

The choice of $U(1)_N$ makes the right-handed neutrino a pure gauge singlet, thus allowing a gauge invariant Majorana mass term enabling a high-scale seesaw mechanism for the generation of neutrino masses. All other matter from complete E_6 matter multiplets survives to low energies, thereby ensuring the cancellation of gauge anomalies.

The three families of E$_6$SSM matter particles fill complete $(\mathbf{27})_i$ representations of the E_6 group, ensuring that full low energy gauge group, including the new $U(1)_N$ gauge symmetry, is anomaly free. In addition to these, the model has two Higgs-like doublets $\hat{H}'$ and $\hat{\bar{H}}'$, the so-called survival Higgs doublets, both originating from extra $(\mathbf{27})'$ and $(\overline{\mathbf{27}})'$ representations to ensure gauge coupling unification at a high scale M_X. The decomposition of the fundamental $(\mathbf{27})$ representation under $SU(5) \times U(1)_N$ and (1) is listed in Tab. 1. All Standard Model fermions as well as their superpartners fit into the multiplets $(\mathbf{10}, 1)_i$ and $(\bar{\mathbf{5}}, 2)_i$. The $(\bar{\mathbf{5}}, -3)$ and $(\mathbf{5}, -2)$ representations contain Higgs-like doublets $\hat{H}_{1i}$, $\hat{H}_{2i}$ and exotic colored

E$_6$SSM states and all new MSSM states have common masses, $T_{\rm E_6SSM}$ and $T_{\rm MSSM}$ respectively. Such scenarios are clearly not realised in the constrained version of the model.

Field	$G_{\rm SM} \times U(1)_N$	$SU(5) \times U(1)_N$	E_6
$\hat{Q}_i = (\hat{Q}_{u_i} \;\; \hat{Q}_{d_i})$	$(\mathbf{3},\mathbf{2},\frac{1}{6},1)_i$	$(\mathbf{10},1)_i$	$(\mathbf{27})_i$
$\hat{u}_i^C$	$(\overline{\mathbf{3}},\mathbf{1},-\frac{2}{3},1)_i$		
$\hat{e}_i^C$	$(\mathbf{1},\mathbf{1},1,1)_i$		
$\hat{d}_i^C$	$(\overline{\mathbf{3}},\mathbf{1},\frac{1}{3},2)_i$	$(\overline{\mathbf{5}},2)_i$	
$\hat{L}_i = (\hat{L}_{\nu_i} \;\; \hat{L}_{e_i})$	$(\mathbf{1},\mathbf{2},-\frac{1}{2},2)_i$		
$\hat{\bar{D}}_i$	$(\overline{\mathbf{3}},\mathbf{1},\frac{1}{3},-3)_i$	$(\overline{\mathbf{5}},-3)_i$	
$\hat{H}_{1i} = (\hat{H}_{1i}^0 \;\; \hat{H}_{1i}^-)$	$(\mathbf{1},\mathbf{2},-\frac{1}{2},-3)_i$		
$\hat{D}_i$	$(\mathbf{3},\mathbf{1},-\frac{1}{3},-2)_i$	$(\mathbf{5},-2)_i$	
$\hat{H}_{2i} = (\hat{H}_{2i}^+ \;\; \hat{H}_{2i}^0)$	$(\mathbf{1},\mathbf{2},\frac{1}{2},-2)_i$		
$\hat{S}_i$	$(\mathbf{1},\mathbf{1},0,5)_i$	$(\mathbf{1},5)_i$	
$\hat{N}_i^C$	$(\mathbf{1},\mathbf{1},0,0)_i$	$(\mathbf{1},0)_i$	
$\hat{H}' = (\hat{H'}^0 \;\; \hat{H'}^-)$	$(\mathbf{1},\mathbf{2},-\frac{1}{2},2)$	$\ni (\overline{\mathbf{5}},2)'$	$\ni (\mathbf{27})'$
$\hat{\bar{H}}' = (\hat{\bar{H}}'^+ \;\; \hat{\bar{H}}'^0)$	$(\mathbf{1},\mathbf{2},\frac{1}{2},-2)$	$\ni (\mathbf{5},-2)'$	$\ni (\overline{\mathbf{27}})'$
$\hat{V}_g^a$	$(\mathbf{8},\mathbf{1},0,0)$	$\ni (\mathbf{24},0)$	$\ni (\mathbf{78})$
$\hat{V}_W^i$	$(\mathbf{1},\mathbf{3},0,0)$	$\ni (\mathbf{24},0)$	$\ni (\mathbf{78})$
$\hat{V}_Y$	$(\mathbf{1},\mathbf{1},0,0)$	$\ni (\mathbf{24},0)$	$\ni (\mathbf{78})$
$\hat{V}_N$	$(\mathbf{1},\mathbf{1},0,0)$	$\ni (\mathbf{1},0)$	$\ni (\mathbf{78})$

Tab. 1: E$_6$SSM SUSY multiplets and their gauge quantum numbers (generation index $i = 1,2,3$), where $G_{\rm SM} \equiv SU(3)_{\rm c} \times SU(2)_{\rm L} \times U(1)_Y$. For the abelian groups $U(1)_Y$ and $U(1)_N$ the charges $Y/2$ and $N/2$ are listed.

matter fields $\hat{D}_i$, $\hat{\bar{D}}_i$. The remaining $SU(5)$ singlets $(\mathbf{1},0)_i$ and $(\mathbf{1},5)_i$ equate to right-handed neutrinos and fields $\hat{S}_i$, respectively. A complete particle listing can be found in Tab. 2.

In an E_6 GUT the gauge bosons and their superpartners fit into the adjoint $(\mathbf{78})$ representation of the E_6, which is decomposed under the low-energy gauge group $SU(3)_{\rm c} \times SU(2)_{\rm L} \times U(1)_Y \times U(1)_N$ into

$$(\mathbf{78}) \to (\mathbf{8},\mathbf{1},0,0) + (\mathbf{1},\mathbf{3},0,0) + (\mathbf{1},\mathbf{1},0,0) + (\mathbf{1},\mathbf{1},0,0) + \cdots \tag{3}$$

The gluons present in a low-energy model are associated to $(\mathbf{8},\mathbf{1},0,0)$. The $(\mathbf{1},\mathbf{3},0,0)$ multiplet contains the weak gauge bosons and the two $U(1)$ gauge fields belong to the two $(\mathbf{1},\mathbf{1},0,0)$ representations. When the E_6 is broken at the GUT scale M_X, the other gauge bosons are expected to have masses of the order of M_X. However,

Superfield	Component fields		
	Spin 0	Spin 1/2	Spin 1
$\hat{Q}_i = (\hat{Q}_{u_i} \;\; \hat{Q}_{d_i})^T$	$\tilde{q}_{iL} = (\tilde{u}_{iL} \;\; \tilde{d}_{iL})^T$	$q_{iL} = (u_{iL} \;\; d_{iL})^T$	
$\hat{u}_i^C$	$\tilde{u}_{iR}^*$	u_{iR}^C	
$\hat{d}_i^C$	$\tilde{d}_{iR}^*$	d_{iR}^C	
$\hat{L}_i = (\hat{L}_{\nu_i} \;\; \hat{L}_{e_i})^T$	$\tilde{\ell}_{iL} = (\tilde{\nu}_{iL} \;\; \tilde{e}_{iL})^T$	$\ell_{iL} = (\nu_{iL} \;\; e_{iL})^T$	
$\hat{e}_i^C$	$\tilde{e}_{iR}^*$	e_{iR}^C	
$\hat{N}_i^C$	$\tilde{\nu}_{iR}^*$	ν_{iR}^C	
$\hat{D}_i$	$\tilde{D}_{iL}$	D_{iL}	
$\hat{\bar{D}}_i$	$\tilde{D}_{iR}^*$	D_{iR}^C	
$\hat{H}_{1i} = (\hat{H}_{1i}^0 \;\; \hat{H}_{1i}^-)^T$	$H_{1i} = (H_{1i}^0 \;\; H_{1i}^-)^T$	$\tilde{H}_{1iL} = (\tilde{H}_{1iL}^0 \;\; \tilde{H}_{1iL}^-)^T$	
$\hat{H}_{2i} = (\hat{H}_{2i}^+ \;\; \hat{H}_{2i}^0)^T$	$H_{2i} = (H_{2i}^+ \;\; H_{2i}^0)^T$	$\tilde{H}_{2iL} = (\tilde{H}_{2iL}^+ \;\; \tilde{H}_{2iL}^0)^T$	
$\hat{S}_i$	S_i	$\tilde{S}_i$	
$\hat{H}' = (\hat{H'}^0 \;\; \hat{H'}^-)^T$	$H' = (H'^0 \;\; H'^-)^T$	$\tilde{H'}_L = (\tilde{H'}_L^0 \;\; \tilde{H'}_L^-)^T$	
$\hat{\bar{H}}' = (\hat{\bar{H}}'^+ \;\; \hat{\bar{H}}'^0)^T$	$\bar{H}' = (\bar{H}'^+ \;\; \bar{H}'^0)^T$	$\tilde{\bar{H}}'_L = (\tilde{\bar{H}}'^+_L \;\; \tilde{\bar{H}}'^0_L)^T$	
$\hat{V}_g^a$		$\tilde{g}^a$	G_μ^a
$\hat{V}_W^i$		$\tilde{W}^i$	W_μ^i
$\hat{V}_Y$		$\tilde{B}$	B_μ
$\hat{V}_N$		$\tilde{Z}'$	Z'_μ

Tab. 2: Component fields of the E$_6$SSM superfields (generation index $i = 1, 2, 3$). The charge conjugation of a spinor ψ is defined as $\psi^C := C\,\bar{\psi}^T$, where $C = i\gamma^2\gamma^0$.

the E$_6$SSM is a low-energy model by construction and does not include these heavy GUT gauge bosons.

As with the MSSM embedded into GUT models, the new bosons absent from the low-energy theory could give rise to significant threshold corrections to gauge coupling unification at M_X. This should be borne in mind when studying the success or failure of gauge coupling unification within a low-energy SUSY model. However the purpose of this paper is to consider the low-energy threshold effects from sparticle masses and to test the significance of these on the physical predictions made by postulates about the high scale parameters.

For $(\mathbf{27})_i$ representations of E_6 the most general renormalizable superpotential with full E_6 invariance is given by the trace of the $(\mathbf{27})_i \times (\mathbf{27})_j \times (\mathbf{27})_k$. Invariance

under the low-energy gauge group allows further terms. But as in the case of the MSSM, the most general gauge invariant superpotential is not phenomenologically viable [2, 8], as it contains baryon number violation and unacceptably large contributions to non-diagonal flavor transitions. To conserve baryon number and avoid flavor changing neutral currents, one first imposes a Z_2^H symmetry, under which all chiral superfields transform as odd, except $\hat{H}_{13}$, $\hat{H}_{23}$ and $\hat{S}_3$.[4] The remaining $SU(3)_{\rm c} \times SU(2)_{\rm L} \times U(1)_Y \times U(1)_N$ and Z_2^H invariant superpotential reads

$$\begin{aligned} W_{\rm E_6SSM} = & -y^e_{ij}(\hat{H}_{13}\hat{L}_i)\hat{e}^C_j - y^d_{ij}(\hat{H}_{13}\hat{Q}_i)\hat{d}^C_j - y^u_{ij}(\hat{Q}_i\hat{H}_{23})\hat{u}^C_j \\ & + \frac{1}{2}M_{ij}\hat{N}^C_i\hat{N}^C_j + h^E_{4j}(\hat{H}_{13}\hat{H}')\hat{e}^C_j + h^N_{4j}(\hat{H}_{23}\hat{H}')\hat{N}^C_j + \mu'(\hat{H}'\hat{\bar{H}}') \\ & + \lambda_i\hat{S}_3(\hat{H}_{1i}\hat{H}_{2i}) + \kappa_i\hat{S}_3\hat{D}_i\hat{\bar{D}}_i + f_{\alpha\beta}\hat{S}_\alpha(\hat{H}_{13}\hat{H}_{2\beta}) + \tilde{f}_{\alpha\beta}\hat{S}_\alpha(\hat{H}_{1\beta}\hat{H}_{23}), \end{aligned} \tag{4}$$

where the $SU(2)$ superfield spinor product is defined as $(AB) := A^2B^1 - A^1B^2$. A problematic consequence of this Z_2^H symmetry would be that the exotic quarks would only have gauge interactions and interactions with the singlet field, leading to stable charged matter in violation of experimental constraints [35, 36, 37]. Therefore the Z_2^H symmetry can only be approximate.

The Z_2^H-violating terms should not lead to rapid proton decay. Hence, another discrete symmetry, analogous to R-parity, must be required. This can be done in two ways: either a Z_2^L symmetry is implemented, under which all superfields except the leptons are even (Model I) or one imposes a Z_2^B symmetry, under which the exotic quarks and leptons are odd whereas the others remain even (Model II). The superpotential (4) is then enlarged by one of the following Z_2^H-violating but $Z_2^{L,B}$-conserving terms

$$W_{\rm Model\ I} = g^Q_{ijk}\hat{D}_i(\hat{Q}_j\hat{Q}_k) + g^q_{ijk}\hat{\bar{D}}_i\hat{d}^C_j\hat{u}^C_k, \tag{5}$$

$$W_{\rm Model\ II} = g^N_{ijk}\hat{N}^C_i\hat{D}_j\hat{u}^C_k + g^E_{ijk}\hat{e}^C_i\hat{D}_j\hat{u}^C_k + g^D_{ijk}(\hat{Q}_i\hat{L}_j)\hat{\bar{D}}_k. \tag{6}$$

In Model I the scalar exotic quarks can decay into two quarks (they are diquarks) and in Model II they are leptoquarks since they decay into a lepton and a quark.

For correct electroweak symmetry breaking only the scalar components of $\hat{H}_{13}$, $\hat{H}_{23}$ and $\hat{S}_3$ get a non-zero VEV. To ensure this, we impose that a certain hierarchy between the Yukawa couplings must exist

$$\kappa_i \sim \lambda_3 \gtrsim \lambda_{1,2} \gg f_{\alpha\beta}, \tilde{f}_{\alpha\beta}, h^E_{4j}, h^N_{4j}. \tag{7}$$

[4] Although a high-scale family structure is not a part of our model by construction, such a Z_2^H symmetry could be the result of a Δ_{27} family symmetry at the GUT scale [15].

This hierarchical structure allows a simplification of the superpotential (4). Integrating out the right-handed neutrinos, which are assumed to be very heavy, and keeping only the dominant terms, one arrives at

$$\begin{aligned} W_{\rm E_6SSM} \approx & -y_\tau(\hat{H}_d\hat{L}_3)\hat{e}_3^C - y_b(\hat{H}_d\hat{Q}_3)\hat{d}_3^C - y_t(\hat{Q}_3\hat{H}_u)\hat{u}_3^C \\ & + \lambda_i\hat{S}(\hat{H}_{1i}\hat{H}_{2i}) + \kappa_i\hat{S}\hat{D}_i\hat{\bar{D}}_i + \mu'(\hat{H}'\hat{\bar{H}}'), \end{aligned} \tag{8}$$

where the scalar components of $\hat{H}_u := \hat{H}_{23}$ and $\hat{H}_d := \hat{H}_{13}$ and $\hat{S} := \hat{S}_3$ develop VEVs, $\langle H_u^0\rangle = v_u/\sqrt{2}$, $\langle H_d^0\rangle = v_d/\sqrt{2}$, giving mass to ordinary matter while $\langle S\rangle = s/\sqrt{2}$ gives exotic quark masses, $\kappa_i S \to \kappa_i s/\sqrt{2} =: \mu_{D_i}$; masses for the fermion components of the first two generations of "inert" Higgs-like doublets (the ones which don't get VEVs) $\mu_{\tilde{H}_\alpha} := \lambda_\alpha s/\sqrt{2}$ and an effective μ-term for the Higgs doublets $\mu_{\rm eff} := \lambda_3 s/\sqrt{2}$. Eq. (8) is the superpotential which will be used in the following analysis to determine the particle spectrum from high scale assumptions, inspired by minimal Supergravity and E_6 GUTs.

The Higgs potential, electroweak symmetry breaking conditions and mass eigenstates of all the particles in the model have been presented in Ref. [8].

3 Threshold corrections in the E$_6$SSM

The E$_6$SSM is a low-energy model which is motivated by a particular high-scale structure. The high and low scales are connected by renormalization group equations which have already been given at the two-loop level in Ref. [8]. In the following we present the results for the threshold corrections which are required for a consistent inclusion of subleading effects. Before presenting our computation and the results we give a brief summary of relevant general features of threshold corrections.

3.1 Threshold corrections for matching full and effective theories

To connect running fundamental E$_6$SSM parameters with SM quantities we consider the SM as an effective theory of the E$_6$SSM and match the two theories at a threshold scale $T_{\rm E_6SSM}$, which should be of the order of the heavy E$_6$SSM particles [38]. To see the need for and the properties of threshold corrections most clearly, we slightly generalize and suppose we have a full and an effective gauge theory and we want to calculate the $\overline{\rm DR}$ gauge coupling $g_{\rm full}(Q_{\rm fix})$ at a fixed scale $Q_{\rm fix}$ in the full theory. As input we know $g_{\rm eff}(Q_{\rm low})$ in the effective theory at some low scale $Q_{\rm low} < Q_{\rm fix}$. We

start with our effective theory at Q_{low} and run the gauge coupling g_{eff} from Q_{low} to the matching scale T_1, using the beta function β_{eff} of the effective theory, see Fig. 1. At T_1 we match the full and the effective theory and calculate $g_{\text{full}}(T_1)$ without the

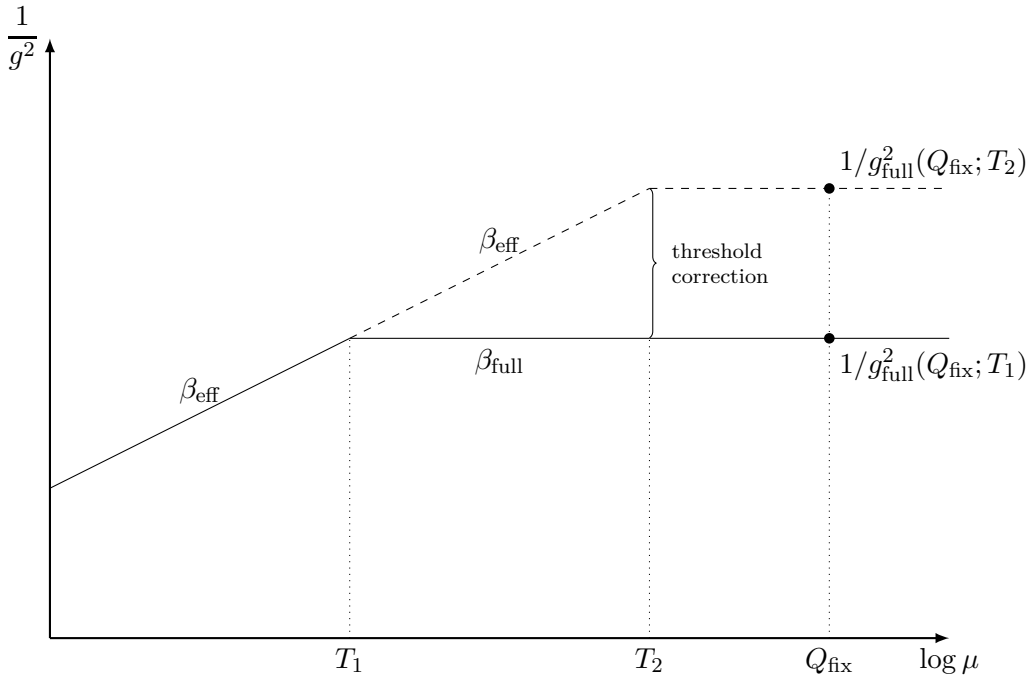

Fig. 1: Visualization of gauge coupling threshold corrections

use of threshold corrections,

$$g_{\text{full}}(T_1) := g_{\text{eff}}(T_1). \tag{9}$$

Now we use the beta functions of the full theory β_{full} to evolve $g_{\text{full}}(T_1)$ to the desired scale Q_{fix} and obtain $g_{\text{full}}(Q_{\text{fix}})$.

The problem with this approach is that the resulting coupling $g_{\text{full}}(Q_{\text{fix}})$ depends on the choice of the unphysical matching scale T_1, i.e. $g_{\text{full}}(Q_{\text{fix}};T_1)$. More precisely, if one would do the same calculation using another matching scale T_2 the difference would be

$$\frac{1}{g^2_{\text{full}}(Q_{\text{fix}};T_1)} - \frac{1}{g^2_{\text{full}}(Q_{\text{fix}};T_2)} = (T_1 - T_2)\frac{2}{(4\pi)^2}\left(\beta_{\text{full}} - \beta_{\text{eff}}\right), \tag{10}$$

because the solution of the RGE is given by

$$\frac{1}{g^2_{\text{full/eff}}(\mu)} = -\frac{2\beta_{\text{full/eff}}}{(4\pi)^2}\log\mu + C. \tag{11}$$

In the limit $T_1 \to T_2$ Eq. (10) becomes

$$\frac{\mathrm{d}}{\mathrm{d}t}\frac{(4\pi)^2}{2g^2_{\text{full}}(Q_{\text{fix}};t)} = \beta_{\text{full}} - \beta_{\text{eff}} \neq 0, \tag{12}$$

which means that the gauge coupling in the full theory at the scale $Q_{\rm fix}$ depends on the unphysical matching scale t and the slope of $g_{\rm full}^{-2}(Q_{\rm fix};t)$ with respect to t is proportional to the difference of the beta functions of the full and the effective theory.

The way out is to use threshold corrections Δg when matching the full and the effective theory, i.e. replace Eq. (9) by

$$g_{\rm full}(T_i) := g_{\rm eff}(T_i) + \Delta g(T_i), \tag{13}$$

where $\Delta g(T_i)$ can be obtained by matching Green functions of the full and the effective theory, see below. As a result the right-hand side of Eq. (12) will vanish, i.e. the gauge coupling $g_{\rm full}(Q_{\rm fix})$ will not depend on the matching scale. This property will be used as a test in Sec. 5.1.

To calculate the threshold corrections we consider a full theory consisting of parameters $\rho_1,\ldots,\rho_p$, light fields $l_1,\ldots,l_q$ and heavy fields $H_1,\ldots,H_r$

$$\mathcal{L}^{\rm full} = \mathcal{L}^{\rm full}(\rho_1,\ldots,\rho_p;l_1,\ldots,l_q,H_1,\ldots,H_r). \tag{14}$$

The effective theory might contain effective parameters $\hat\rho_1,\ldots,\hat\rho_k$ and effective light fields $\hat l_1,\ldots,\hat l_q$, where the heavy fields were integrated out

$$\mathcal{L}^{\rm eff} = \mathcal{L}^{\rm eff}(\hat\rho_1,\ldots,\hat\rho_k;\hat l_1,\ldots,\hat l_q). \tag{15}$$

The requirement that both the full and the effective theory describe the same physics in the limit $p\to 0$ can be achieved by equating all connected Green functions with light external fields l_i in the full and in the effective theory at zero external momenta. This condition leads to the equality of all one-particle irreducible correlation functions Γ that are one-particle irreducible with respect to the light fields l_i (1LPI)

$$\Gamma^{\rm full}_{l_{i_1}l_{i_2}\cdots l_{i_n}}(\rho_1,\ldots,\rho_p)\Big|_{k_i=0} = \Gamma^{\rm eff}_{l_{i_1}l_{i_2}\cdots l_{i_n}}(\hat\rho_1,\ldots,\hat\rho_k)\Big|_{k_i=0}, \tag{16}$$

where k_i are the momenta of the external fields. The next step is to decompose the renormalized 1LPI correlation functions into a tree-level part and a part which contains one-loop contributions

$$\Gamma^{\rm full}_{l_{i_1}l_{i_2}\cdots l_{i_n}} = \Gamma^{\rm full,tree}_{l_{i_1}l_{i_2}\cdots l_{i_n}} + \Gamma^{\rm full,1L}_{l_{i_1}l_{i_2}\cdots l_{i_n}}, \tag{17}$$

$$\Gamma^{\rm eff}_{l_{i_1}l_{i_2}\cdots l_{i_n}} = \Gamma^{\rm eff,tree}_{l_{i_1}l_{i_2}\cdots l_{i_n}} + \Gamma^{\rm eff,1L}_{l_{i_1}l_{i_2}\cdots l_{i_n}}. \tag{18}$$

Imposing a relative field renormalization for the renormalized fields in the full and effective theory

$$\hat l_i = \left(1+\frac{1}{2}K_{l_i}\right) l_i, \qquad\qquad (i=1,\ldots,q) \tag{19}$$

and inserting Eq. (17)–(19) into (16) yields the matching condition

$$\Gamma^{\text{full,tree}}_{l_{i_1}l_{i_2}\cdots l_{i_n}} + \Gamma^{\text{full,1L}}_{l_{i_1}l_{i_2}\cdots l_{i_n}} = \left(1 + \frac{1}{2}\sum_{n=1}^{q} K_{l_{i_n}}\right)\Gamma^{\text{eff,tree}}_{\hat{l}_{i_1}\hat{l}_{i_2}\cdots\hat{l}_{i_n}} + \Gamma^{\text{eff,1L}}_{\hat{l}_{i_1}\hat{l}_{i_2}\cdots\hat{l}_{i_n}} + O(\hbar^2). \tag{20}$$

This equation is evaluated at zero external momenta. The analogous equation holds for the derivatives of the 1LPI correlation functions. Imposing all matching conditions yields the definitions for the K_{l_i} in terms of 1LPI correlation functions and at the same time the desired relations between the parameters of the effective and full theory (threshold corrections)

$$\hat{\rho}_i = \rho_i + \Delta\rho_i^{(\text{1-loop})}(\rho_1, \ldots, \rho_p, K_{l_1}, \ldots, K_{l_q}), \qquad (i = 1, \ldots, k). \tag{21}$$

3.2 Gauge coupling threshold corrections in the E_6SSM

Strong gauge coupling To calculate the threshold correction for the gauge coupling g_3 of the unbroken $SU(3)_c$ one needs to apply the matching procedure of Sec. 3.1 to the following 1LPI correlation functions

$$\partial_p\, \Gamma^{\text{E}_6\text{SSM}}_{q_i\bar{q}_i}(p,-p)\big|_{p=0} = \partial_p\, \Gamma^{\text{SM}}_{q_i\bar{q}_i}(p,-p)\big|_{p=0}\,, \tag{22}$$

$$\partial_{k^2}\, \Gamma^{\text{E}_6\text{SSM}}_{G^a_\mu G^b_\nu}(k,-k)\Big|_{k^2=0} = \partial_{k^2}\, \Gamma^{\text{SM}}_{G^a_\mu G^b_\nu}(k,-k)\Big|_{k^2=0}\,, \tag{23}$$

$$\Gamma^{\text{E}_6\text{SSM}}_{G^a_\mu q_i\bar{q}_i}(k,p,-(p+k))\Big|_{p=k=0} = \Gamma^{\text{SM}}_{G^a_\mu q_i\bar{q}_i}(k,p,-(p+k))\Big|_{p=k=0}\,, \tag{24}$$

where q_i are the light colored fields that remain in the SM, i.e. the SM quarks. After imposing the relative field renormalizations (19) and decomposing the 1LPI functions into a tree-level and a loop part one gets the threshold correction for g_3

$$g_3^{\overline{\text{MS}},\text{SM}} = g_3^{\overline{\text{MS}},\text{E}_6\text{SSM}} + \frac{g_3^3}{(4\pi)^2}\left(\sum_f \frac{4}{3}F_f C(r_f)\log\frac{m_f}{\mu} + \sum_s \frac{1}{3}F_s C(r_s)\log\frac{m_s}{\mu}\right). \tag{25}$$

The sums run over all heavy fermions f and scalars s that are integrated out. Eq. (25) is also in agreement with the general result in [39]. The constants $C(r)$ are invariants of the representations r of $SU(3)_c$ and are given by

$$C(N) = \frac{1}{2} \qquad \text{(fundamental representation } N\text{)}, \tag{26}$$

$$C(G) = 3 \qquad \text{(adjoint representation } G\text{)}, \tag{27}$$

and F_f, F_s account for the different number of field degrees of freedom

$$F_f = \begin{cases} 1 & \text{if } f \text{ is a Dirac fermion,} \\ 1/2 & \text{if } f \text{ is a Majorana fermion,} \end{cases} \tag{28}$$

$$F_s = \begin{cases} 1 & \text{if } s \text{ is a complex scalar,} \\ 1/2 & \text{if } s \text{ is a real scalar.} \end{cases} \tag{29}$$

When matching the E_6SSM to the SM, only the gluino, the squarks and the exotics contribute in Eq. (25) and we have

$$C(r_{\tilde{g}}) = C(G) = 3, \qquad C(r_{\tilde{q}_{ik}}) = C(r_{\tilde{D}_{ik}}) = C(r_{D_i}) = C(N) = 1/2, \tag{30}$$

$$F_{\tilde{g}} = 1/2, \qquad F_{\tilde{q}_{ik}} = F_{\tilde{D}_{ik}} = F_{D_i} = 1. \tag{31}$$

Then the threshold correction (25) reduces to

$$\begin{aligned} g_3^{\overline{\rm DR},\rm E_6SSM} = g_3^{\overline{\rm MS},\rm SM} + \frac{g_3^3}{(4\pi)^2}\Bigg[\frac{1}{2} - 2\log\frac{m_{\tilde{g}}}{\mu} - \frac{1}{6}\sum_{\tilde{q}\in\{\tilde{u},\tilde{d}\}}\sum_{i=1}^{3}\sum_{k=1}^{2}\log\frac{m_{\tilde{q}_{ik}}}{\mu} \\ - \frac{2}{3}\sum_{i=1}^{3}\log\frac{m_{D_i}}{\mu} - \frac{1}{6}\sum_{i=1}^{3}\sum_{k=1}^{2}\log\frac{m_{\tilde{D}_{ik}}}{\mu}\Bigg], \end{aligned} \tag{32}$$

where we have added a finite counterterm which converts g_3 from the $\overline{\rm MS}$ to the $\overline{\rm DR}$ scheme [40].

Electroweak gauge couplings The calculation of threshold corrections for the couplings g_Y and g_2 is more involved, because the gauge group $SU(2)_{\rm L} \times U(1)_Y$ is spontaneously broken to $U(1)_{\rm em}$. From the relations

$$g_Y = \frac{e}{c_W}, \qquad g_2 = \frac{e}{s_W}, \qquad c_W = \frac{m_W}{m_Z} \tag{33}$$

one can see that the threshold corrections for g_Y and g_2 are related to those of the $W^\pm$ and Z boson masses as well as to the gauge coupling e of the remaining $U(1)_{\rm em}$ gauge symmetry. Therefore the following matching conditions are imposed to obtain threshold corrections for e, m_Z and m_W

$$\partial_{k^2}^n\, \Gamma^{\rm E_6SSM}_{W_\mu^+ W_\nu^-}(k,-k)\Big|_{k^2=0} = \partial_{k^2}^n\, \Gamma^{\rm SM}_{W_\mu^+ W_\nu^-}(k,-k)\Big|_{k^2=0} \qquad (n=0,1), \tag{34}$$

$$\partial_{k^2}^n\, \Gamma^{\rm E_6SSM}_{Z_\mu Z_\nu}(k,-k)\Big|_{k^2=0} = \partial_{k^2}^n\, \Gamma^{\rm SM}_{Z_\mu Z_\nu}(k,-k)\Big|_{k^2=0} \qquad (n=0,1), \tag{35}$$

$$\partial_{k^2}\, \Gamma^{\rm E_6SSM}_{A_\mu A_\nu}(k,-k)\Big|_{k^2=0} = \partial_{k^2}\, \Gamma^{\rm SM}_{A_\mu A_\nu}(k,-k)\Big|_{k^2=0}, \tag{36}$$

$$\Gamma^{\rm E_6SSM}_{Z_\mu A_\nu}(k,-k)\Big|_{k^2=0} = \Gamma^{\rm SM}_{Z_\mu A_\nu}(k,-k)\Big|_{k^2=0}, \tag{37}$$

$$\partial_p\, \Gamma^{\rm E_6SSM}_{\psi_{Li}\bar{\psi}_{Lj}}(p,-p)\Big|_{p=0} = \partial_p\, \Gamma^{\rm SM}_{\psi_{Li}\bar{\psi}_{Lj}}(p,-p)\Big|_{p=0}, \tag{38}$$

$$\partial_p\, \Gamma^{\rm E_6SSM}_{\psi_{Ri}\bar{\psi}_{Rj}}(p,-p)\Big|_{p=0} = \partial_p\, \Gamma^{\rm SM}_{\psi_{Ri}\bar{\psi}_{Rj}}(p,-p)\Big|_{p=0}, \tag{39}$$

$$\Gamma^{\rm E_6SSM}_{A_\mu\psi_i\bar{\psi}_j}(k,p,-(p+k))\Big|_{k=p=0} = \Gamma^{\rm SM}_{A_\mu\psi_i\bar{\psi}_j}(k,p,-(p+k))\Big|_{k=p=0}. \tag{40}$$

The additional matching condition for $\Gamma_{Z_\mu A_\nu}$ is necessary, because the gauge fields B_μ, $\vec{W}_\mu$ mix to A_μ, Z_μ and $W_\mu^\pm$. Introducing relative field renormalizations for $W_\mu^\pm$, Z_μ, A_μ, ψ_{iL} and ψ_{iR} and inserting them into the matching conditions (34)–(40) leads to the threshold corrections for the W and Z boson masses and the electromagnetic coupling[5]

$$(m_V^{\rm SM})^2 = (m_V^{\rm E_6SSM})^2 + \Gamma^{\rm E_6SSM,1L,heavy}_{V_\mu V_\nu,T}\Big|_{k^2=0} - m_V^2 K_{VV}, \qquad V \in \{W,Z\}, \tag{41}$$

$$\equiv (m_V^{\rm E_6SSM})^2 + \Delta m_V^2, \tag{42}$$

$$e^{\rm SM} = e^{\rm E_6SSM}\left(1 - \frac{1}{2}K_{AA} - \frac{s_W}{2c_W}K_{ZA}\right) \equiv e^{\rm E_6SSM} + \Delta e. \tag{43}$$

The relative field renormalization constants in Eq. (41) and (43) are given by

$$K_{AA} = -\frac{\partial}{\partial k^2}\,\Gamma^{\rm E_6SSM,1L,heavy}_{A_\mu A_\nu,T}\Big|_{k^2=0}, \qquad K_{ZA} = \frac{2}{m_Z^2}\,\Gamma^{\rm E_6SSM,1L,heavy}_{A_\mu Z_\nu,T}\Big|_{k^2=0}, \tag{44}$$

$$K_{WW} = -\frac{\partial}{\partial k^2}\,\Gamma^{\rm E_6SSM,1L,heavy}_{W_\mu^+ W_\nu^-,T}\Big|_{k^2=0}, \qquad K_{ZZ} = -\frac{\partial}{\partial k^2}\,\Gamma^{\rm E_6SSM,1L,heavy}_{Z_\mu Z_\nu,T}\Big|_{k^2=0} \tag{45}$$

and by $\Gamma^{\rm E_6SSM,1L,heavy}_{V_\mu V'_\nu,T}$ we denote the one-loop parts of the gauge boson 2-point functions that contain all particles that we integrate out, i.e. all non-SM particles. Using Eq. (41)–(43) one can write the threshold corrections for g_Y and g_2 in the form

$$g_Y^{\rm SM} = \frac{e^{\rm SM}}{c_W^{\rm SM}} = \frac{e^{\rm SM}\, m_Z^{\rm SM}}{m_W^{\rm SM}} = g_Y^{\rm E_6SSM}\left(1 + \frac{\Delta e}{e} + \frac{1}{2}\frac{\Delta m_Z^2}{m_Z^2} - \frac{1}{2}\frac{\Delta m_W^2}{m_W^2}\right), \tag{46}$$

$$g_2^{\rm SM} = \frac{e^{\rm SM}}{s_W^{\rm SM}} = \frac{e^{\rm SM}}{\sqrt{1 - \left(\frac{m_W^{\rm SM}}{m_Z^{\rm SM}}\right)^2}} = g_2^{\rm E_6SSM}\left(1 + \frac{\Delta e}{e} - \frac{c_W^2}{s_W^2}\frac{\Delta m_Z^2}{2m_Z^2} + \frac{c_W^2}{s_W^2}\frac{\Delta m_W^2}{2m_W^2}\right). \tag{47}$$

Inserting the explicit form of Δe, Δm_W^2 and Δm_Z^2 yields

$$\begin{aligned} g_Y^{\overline{\rm DR},\rm E_6SSM} = g_Y^{\overline{\rm MS},\rm SM} + \frac{g_Y^3}{(4\pi)^2}\Bigg[& -\frac{4}{3}N_c\sum_{i=1}^{3}\left(\frac{Y_{D_i}}{2}\right)^2 \log\frac{m_{D_i}}{\mu} \\ & -\frac{1}{3}N_c\sum_{i=1}^{3}\sum_{k=1}^{2}\left(\frac{Y_{\tilde{D}_{ik}}}{2}\right)^2 \log\frac{m_{\tilde{D}_{ik}}}{\mu} \\ & -\frac{1}{3}N_c\sum_{i=1}^{3}\sum_{k=L,R}\left\{\left(\frac{Y_{\tilde{u}_{ik}}}{2}\right)^2 \log\frac{m_{\tilde{u}_{ik}}}{\mu} + \left(\frac{Y_{\tilde{d}_{ik}}}{2}\right)^2 \log\frac{m_{\tilde{d}_{ik}}}{\mu}\right\} \\ & -\frac{1}{3}\sum_{i=1}^{3}\sum_{k=L,R}\left(\frac{Y_{\tilde{e}_{ik}}}{2}\right)^2 \log\frac{m_{\tilde{e}_{ik}}}{\mu} - \frac{1}{3}\sum_{i=1}^{3}\left(\frac{Y_{\tilde{\nu}_{iL}}}{2}\right)^2 \log\frac{m_{\tilde{\nu}_{iL}}}{\mu} \end{aligned}$$

[5]The Ward identity which reflects the $U(1)_{\rm em}$ gauge invariance in the Standard Model was used to simplify the result.

$$
\begin{aligned}
&- \frac{1}{3}\sum_{i=1}^{2}\sum_{p=1}^{2}\sum_{j=1}^{2}\left(\frac{Y_{H^j_{pi}}}{2}\right)^2 \log\frac{m_{H^j_{pi}}}{\mu} - \frac{1}{3}\sum_{j=1}^{2}\left(\frac{Y_{H^j_{23}}}{2}\right)^2 \log\frac{m_H}{\mu} \\
&- \frac{2}{3}\sum_{i=1}^{3}\sum_{p=1}^{2}\sum_{j=1}^{2}\left(\frac{Y_{\tilde{H}^j_{piL}}}{2}\right)^2 \log\frac{m_{\tilde{H}^j_{piL}}}{\mu} \\
&- \frac{1}{3}\sum_{j=1}^{2}\left(\frac{Y_{H'^j}}{2}\right)^2 \log\frac{m_{H'^j}}{\mu} - \frac{2}{3}\sum_{j=1}^{2}\left(\frac{Y_{\tilde{H}'^j_L}}{2}\right)^2 \log\frac{m_{\tilde{H}'^j_L}}{\mu} \\
&- \frac{1}{3}\sum_{j=1}^{2}\left(\frac{Y_{\bar{H}'^j}}{2}\right)^2 \log\frac{m_{\bar{H}'^j}}{\mu} - \frac{2}{3}\sum_{j=1}^{2}\left(\frac{Y_{\tilde{\bar{H}}'^j_L}}{2}\right)^2 \log\frac{m_{\tilde{\bar{H}}'^j_L}}{\mu}\Bigg], \qquad (48)
\end{aligned}
$$

$$
\begin{aligned}
g_2^{\overline{\rm DR},\rm E_6SSM} = g_2^{\overline{\rm MS},\rm SM} + \frac{g_2^3}{(4\pi)^2}\Bigg[&\frac{1}{3} - \frac{1}{6}N_c\sum_{i=1}^{3}\log\frac{m_{\tilde{q}_{iL}}}{\mu} - \frac{1}{6}\sum_{i=1}^{3}\log\frac{m_{\tilde{\ell}_{iL}}}{\mu} \\
&- \frac{4}{3}\log\frac{m_{\tilde{W}}}{\mu} - \frac{1}{6}\log\frac{m_H}{\mu} \\
&- \frac{1}{6}\sum_{i=1}^{2}\sum_{p=1}^{2}\log\frac{m_{H_{pi}}}{\mu} - \frac{1}{3}\sum_{i=1}^{3}\sum_{p=1}^{2}\log\frac{m_{\tilde{H}_{piL}}}{\mu} \\
&- \frac{1}{6}\log\frac{m_{H'}}{\mu} - \frac{1}{3}\log\frac{m_{\tilde{H'}_L}}{\mu} \\
&- \frac{1}{6}\log\frac{m_{\bar{H}'}}{\mu} - \frac{1}{3}\log\frac{m_{\tilde{\bar{H}}'_L}}{\mu}\Bigg], \qquad (49)
\end{aligned}
$$

where we have added a finite counterterm which converts g_2 from the $\overline{\rm MS}$ to the $\overline{\rm DR}$ scheme [40] and neglected mixing.

3.3 Yukawa couplings in the E$_6$SSM

Since the SM fermion masses are measured but not the Yukawa couplings, we don't define the E$_6$SSM Yukawa couplings in terms of threshold corrections to the running SM Yukawa couplings. Instead we directly match them at the one-loop level to the measured SM fermion masses and gauge couplings via

$$
y_t^{\overline{\rm DR},\rm E_6SSM} = \frac{g_2^{\overline{\rm DR},\rm E_6SSM} m_t^{\text{on-shell,SM}}}{\sqrt{2} m_W^{\text{on-shell,SM}} \sin\beta}\left(1 - \frac{\delta m_W}{m_W^{\text{on-shell,SM}}} + \frac{\delta m_t}{m_t^{\text{on-shell,SM}}}\right), \qquad (50)
$$

$$
y_b^{\overline{\rm DR},\rm E_6SSM} = \frac{g_2^{\overline{\rm DR},\rm E_6SSM} m_b^{\overline{\rm DR},(5)}(m_Z)}{\sqrt{2} m_W^{\text{on-shell,SM}} \cos\beta}\left(1 - \frac{\delta m_W}{m_W^{\text{on-shell,SM}}} + \frac{\delta m_b - \delta m_b^{(5)} + \delta m_b^{\text{shift}}}{m_b^{\overline{\rm DR},(5)}(m_Z)}\right), \qquad (51)
$$

$$
y_\tau^{\overline{\rm DR},\rm E_6SSM} = \frac{g_2^{\overline{\rm DR},\rm E_6SSM} m_\tau^{\text{on-shell,SM}}}{\sqrt{2} m_W^{\text{on-shell,SM}} \cos\beta}\left(1 - \frac{\delta m_W}{m_W^{\text{on-shell,SM}}} + \frac{\delta m_\tau}{m_\tau^{\text{on-shell,SM}}}\right). \qquad (52)
$$

Here $m_t^{\text{on-shell,SM}}$, $m_\tau^{\text{on-shell,SM}}$ and $m_W^{\text{on-shell,SM}}$ are Standard Model on-shell masses [41]. To avoid large logarithms from the bottom mass we use the $\overline{\text{DR}}$ value of m_b in the 5-flavor QCD at m_Z, $m_b^{\overline{\text{DR}},(5)}(m_Z) = 2.83$ GeV [42] which we then shift to the scale μ where the Yukawa couplings are evaluated at. The counterterms in Eqs. (50)–(52) are defined as

$$\delta m_f = \delta m_f^{\text{on-shell,E}_6\text{SSM}} - \delta m_f^{\overline{\text{DR}},\text{E}_6\text{SSM}} = \widetilde{\Re\text{e}}\,\Sigma_f(m_f^2)\Big|_{\text{finite}} \qquad (f = t, b, \tau), \tag{53}$$

$$\delta m_b^{(5)} = \delta m_b^{\text{on-shell,QCD(5)}} - \delta m_b^{\overline{\text{DR}},(5)} = -\frac{4m_b^{\overline{\text{DR}},(5)}(m_Z)}{3(4\pi)^2} g_3^2 \left(5 + 3\log\frac{\mu^2}{m_b^2}\right), \tag{54}$$

$$\delta m_b^{\text{shift}} = \beta_{m_b}^{\overline{\text{DR}},(5)} \log\frac{\mu}{m_Z} = -2m_b^{\overline{\text{DR}},(5)}(m_Z)\frac{g_3^2}{4\pi^2}\log\frac{\mu}{m_Z}, \tag{55}$$

$$\delta m_W = \delta m_W^{\text{on-shell,E}_6\text{SSM}} - \delta m_W^{\overline{\text{DR}},\text{E}_6\text{SSM}} = \widetilde{\Re\text{e}}\,\Pi_{WW,T}(m_W^2)\Big|_{\text{finite}}. \tag{56}$$

The self-energies Σ_f and $\Pi_{WW,T}$ are listed in Appendix C. It was checked that the divergences of (50)–(52), see Appendix D, are in agreement with the prediction from the one-loop RGEs.

4 Obtaining accurate spectra in the CE$_6$SSM

4.1 The CE$_6$SSM and its parameters

The threshold corrections presented in the previous section improve the precision of the high-scale–low-scale connection in the general E$_6$SSM. In the present paper we apply them to the constrained version of the E$_6$SSM (CE$_6$SSM). The CE$_6$SSM is defined by a universal scalar mass m_0, gaugino mass $M_{1/2}$ and trilinear mass A at the gauge coupling unification scale M_X [8, 9]. Owing to the unification of matter and Higgs fields in complete GUT multiplets these constraints are particularly well motivated. The soft scalar masses from the survival Higgs (which appear in the incomplete $(\mathbf{27})'$ and $(\overline{\mathbf{27}})'$ representations) sector, $m_{H'}$, $m_{\bar{H}'}$ are not assumed to be unified with m_0 and the soft bilinear $B\mu'$ is also unconstrained.

The CE$_6$SSM is an example of a highly predictive, non-minimal SUSY model. It contains many new states at the TeV scale but has only few free parameters. In theory, the CE$_6$SSM is fully determined by specifying the gauge couplings, the superpotential parameters $y_{t,b,\tau}$, λ_i and κ_i and the universal soft parameters m_0, $M_{1/2}$, A at the GUT scale as well as the survival Higgs parameters. All high-scale parameters are shown in the top row of boxes in Fig. 2.

In practice, the model predictions of course need to agree with known SM constraints, in particular with the four known masses m_Z, $m_{t,b,\tau}$ and the known low-

energy gauge couplings. Furthermore, it is useful to take the low-energy values of $\tan\beta = v_u/v_d$ and $s = \sqrt{2}\langle S\rangle$ as free parameters of the model. In this way, the six GUT-scale parameters m_0, $M_{1/2}$, A and $y_{t,b,\tau}$ are traded for the four known SM mass constraints and the two low-scale input parameters $\tan\beta$ and s. Compared to the familiar CMSSM, the CE$_6$SSM has no μ and $B\mu$ parameters, which could be adjusted to fulfill SM constraints. Hence, the CMSSM input parameters m_0, $M_{1/2}$ and A are calculable in the CE$_6$SSM.

Fig. 2 shows the resulting structure of input and output of the CE$_6$SSM and the connection of the high and low scales. High-scale input parameters are the superpotential parameters $\lambda_i(M_X)$ and $\kappa_i(M_X)$; low-scale input parameters are $s(Q_{\rm fix})$, $\tan\beta(Q_{\rm fix})$ and the survival Higgs parameters (defined at the matching scale $T_{\rm E_6SSM}$), all defined in the $\overline{\rm DR}$ scheme. The low-scale SM constraints fix the remaining parameters. In previous studies λ_i, κ_i, s and $\tan\beta$ were sufficient to fix the spectrum. Here, with the inclusion of threshold corrections, we will be able to study the perturbation caused by the survival Higgs sector as well.

As the Figure shows, $6 + 3 + 4 = 13$ high-scale parameters have been traded against these 13 low-scale input parameters, so this high- and low-scale input determines the structure of the model completely and at all scales. The fixed scale $Q_{\rm fix}$, where s and $\tan\beta$ are defined at, is set in Sec. 5 to a value of the order of the matching scale $T_{\rm E_6SSM}$.

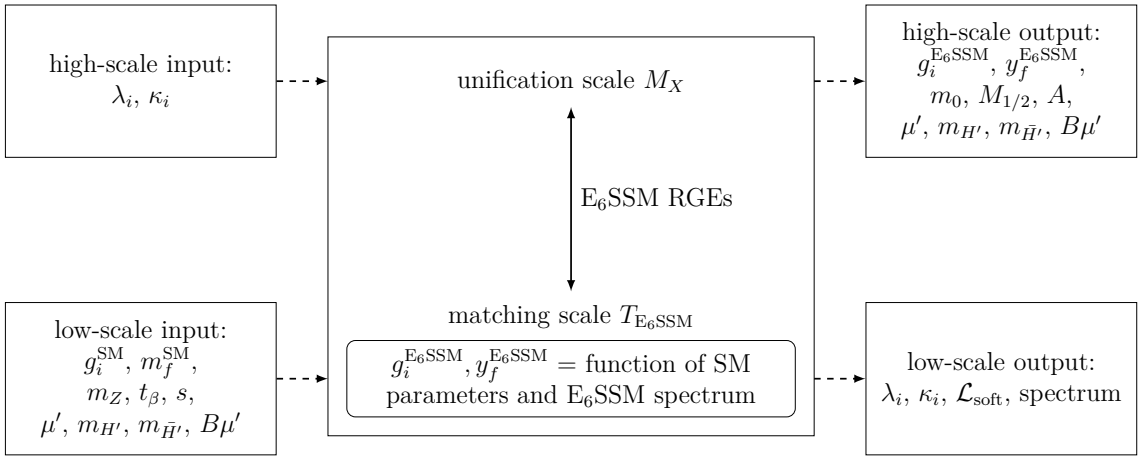

Fig. 2: The structure of high- and low-scale input and output of the CE$_6$SSM.

4.2 Numerical procedure and the improved spectrum generator

We extended the particle spectrum generator previously written for [8], which is partly based on SOFTSUSY 2.0.5 [24]. As input the program gets a CE$_6$SSM parameter point specified by the high- and low-scale input

$$\begin{aligned} &\lambda_{1,2,3}(M_X), \kappa_{1,2,3}(M_X), s(Q_{\rm fix}), \tan\beta(Q_{\rm fix}), \\ &\mu'(T_{\rm E_6SSM}), m_{H'}(T_{\rm E_6SSM}), m_{\bar{H}'}(T_{\rm E_6SSM}), B\mu'(T_{\rm E_6SSM}), \end{aligned} \tag{57}$$

and the program knows about the SM constraints discussed above. As illustrated in Fig. 2, RGEs and threshold corrections connect high and low scales, and the aim is to find output parameters consistent with the given input and then to compute the physical particle masses from the obtained low-energy SUSY breaking parameters. However, the threshold corrections can only be computed once the full mass spectrum is known. Hence, these steps need to be iterated until convergence is reached, and in the first iteration the threshold corrections must be ignored.

In the actual computation, we divide the basic strategy of each iteration into five steps, see Fig. 3. The details are as follows.

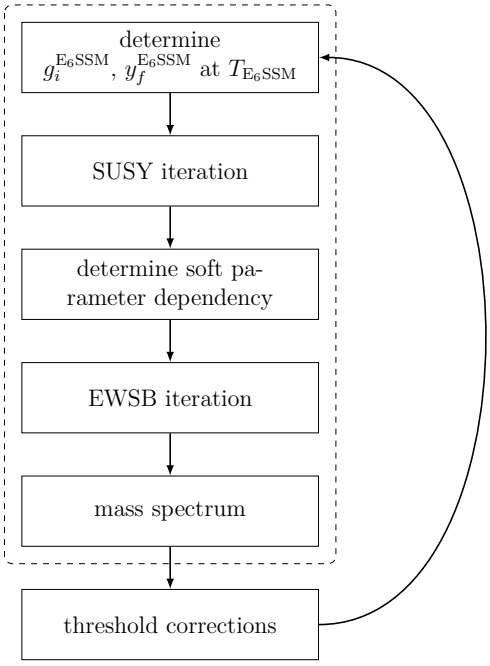

Fig. 3: Program flow chart. The dashed box marks the structure of the old spectrum generator, which had no threshold corrections.

1. Determine the gauge and Yukawa couplings in the E$_6$SSM at the threshold

scale $T_{\mathrm{E_6SSM}}$ from the known SM gauge couplings and masses, using SM RGEs and the threshold corrections.

(a) Evolve the SM $\overline{\mathrm{MS}}$ gauge and Yukawa couplings from their known values at m_Z [41] to the intermediate matching scale $T_{\mathrm{E_6SSM}}$ using SM RGEs.

(b) Convert the SM $\overline{\mathrm{MS}}$ couplings to $\mathrm{E_6SSM}$ $\overline{\mathrm{DR}}$ couplings using the individual particle threshold corrections discussed in Sec. 3. This step is only possible once the physical particle masses are known, i.e. after the first iteration. Hence, in the first iteration, the threshold corrections are replaced by the trivial definitions

$$y_f^{\mathrm{E_6SSM}} := \frac{y_f^{\mathrm{SM}}}{\cos\beta}\ (f = b, \tau), \qquad y_t^{\mathrm{E_6SSM}} := \frac{y_t^{\mathrm{SM}}}{\sin\beta}, \tag{58}$$

$$g_i^{\overline{\mathrm{DR}},\mathrm{E_6SSM}} := g_i^{\overline{\mathrm{MS}},\mathrm{SM}}\ (i = 1, 2, 3). \tag{59}$$

Note that, in contrast to Ref. [8], we do not use an intermediate matching to the MSSM because the MSSM and the $\mathrm{E_6SSM}$ spectra are typically mixed.

2. Use RGEs to determine the high-scale gauge and Yukawa couplings and the low-scale values of the λ_i, κ_i. This step is completely independent of all soft SUSY breaking parameters because of the structure of the RGEs.

(a) Estimate low-energy values for the Yukawa couplings $\lambda_i(T_{\mathrm{E_6SSM}})$, $\kappa_i(T_{\mathrm{E_6SSM}})$. The necessity of this estimate is an additional complication not present e.g. in the CMSSM. The difference is due to the fact that in the CMSSM all high-scale input parameters are soft breaking parameters, while here they are superpotential parameters.

(b) Evolve all $\mathrm{E_6SSM}$ gauge and Yukawa couplings from $T_{\mathrm{E_6SSM}}$ up to the unification scale M_X, defined as the scale where $g_1 = g_2$, using two-loop $\mathrm{E_6SSM}$ RGEs.

(c) Set Yukawa couplings $\lambda_i(M_X)$, $\kappa_i(M_X)$ to program input values.

(d) Set $g_N := g_0/\sqrt{40}$, where g_0 is defined by $g_1(M_X)$.

(e) Perform an iteration between M_X and $T_{\mathrm{E_6SSM}}$ to obtain values for the gauge and Yukawa couplings and λ_i, κ_i until consistency is reached with low-energy boundary conditions $y_f(T_{\mathrm{E_6SSM}})$, $g_i(T_{\mathrm{E_6SSM}})$ and high energy boundary conditions $\lambda_i(M_X)$, $\kappa_i(M_X)$.

3. With the gauge, Yukawa and λ_i, κ_i couplings now known at all scales we find solutions for the soft breaking parameters. They are determined by the high-scale constraints of universal m_0, $M_{1/2}$, A, and by low-scale electroweak symmetry breaking (EWSB) conditions, i.e. consistency with the measured value of m_Z and the input values for $\tan\beta$ and s. First, the dependency of the low-energy soft mass parameters on the GUT scale values m_0^2, $M_{1/2}$, A_0 is expressed in terms of the semi-analytical formulas

$$m_i^2(t) = a_i(t)m_0^2 + b_i(t)M_{1/2}^2 + c_i(t)A_0M_{1/2} + d_i(t)A_0^2, \tag{60}$$

$$A_i(t) = e_i(t)A_0 + f_i(t)M_{1/2}, \tag{61}$$

$$M_i(t) = p_i(t)A_0 + q_i(t)M_{1/2}, \tag{62}$$

where the coefficients $a_i(t), \ldots, q_i(t)$ are calculated numerically at the scale $t = \log T_{\mathrm{E_6SSM}}/M_X$.

4. Next, the EWSB conditions are used to fix the values of the soft parameters.

   (a) The obtained expressions for the low-energy soft parameters $m_i^2(t)$, $M_i(t)$, $A_i(t)$ are then combined with tree level EWSB conditions

   $$\frac{\partial V}{\partial v_1} = \frac{\partial V}{\partial v_2} = \frac{\partial V}{\partial s} = 0 \tag{63}$$

   and the known values of m_Z, $\tan\beta$ and s to form three quadratic equations in the soft masses m_0, $M_{1/2}$ and A, which can be reduced to a single quartic equation.

   (b) This quartic equation is then solved numerically and the values used to determine the mass spectra. Note that in principle there will be four solutions, though some or all may be complex. Therefore our routine deals with between zero and four sets of real solutions.

   (c) Tadpole corrections can now be calculated and added to the EWSB conditions, and a solution of consistent EWSB for the leading one-loop effective potential is found iteratively.

5. The full $\mathrm{CE_6SSM}$ particle mass spectrum is now determined for each set of $\{m_0^2, M_{1/2}, A_0\}$ found to be consistent with both high scale and low scale boundary conditions.

The final solution is found by iterating over all five steps until convergent solutions are obtained.

It is important to note that in general EWSB is not guaranteed in the CE$_6$SSM, i.e. solutions for $\{m_0^2, M_{1/2}, A_0\}$ from Eq. (63) are not always found. But for sufficiently large values of κ_i the soft parameter m_S^2 always gets negative at low energies, which triggers EWSB [8].

5 Results

In this section we present the results obtained with our improved CE$_6$SSM spectrum generator. We start by quantifying how the threshold corrections stabilize the results for parameters like gauge couplings and the mass spectrum. We will then extensively discuss the resulting, more accurate mass spectrum. On the one hand we will obtain more precise information on previously defined benchmark points, implying that some are now excluded by LHC data. On the other hand we scan over the parameter space and find large regions which are compatible with LHC limits on SUSY particles and are consistent with the latest discovery of the new boson which we associate with the lightest Higgs boson in the model. Finally we investigate the impact of the survival Higgs sector, which is possible due to the threshold corrections. It has implications on gauge coupling unification and on the predictions for the low-energy mass spectrum. In subsequent studies we sometimes make use of a test point, PP1, to illustrate effects, which is defined by,

$$\begin{aligned} \tan\beta(Q_{\rm fix}) = 35, \lambda_{1,2,3}(M_X) = \kappa_{1,2,3}(M_X) = 0.2, s(Q_{\rm fix}) = 10 \text{ TeV}, \\ \mu'(T_{\rm E_6SSM}) = m_{H'}(T_{\rm E_6SSM}) = m_{\bar{H}'}(T_{\rm E_6SSM}) = 10 \text{ TeV}, B\mu'(T_{\rm E_6SSM}) = 0. \end{aligned} \tag{64}$$

Furthermore we set $Q_{\rm fix} = 3$ TeV for all the following analyses.

5.1 Matching scale dependency

In Sec. 3.1 we presented Fig. 1 to illustrate how the threshold corrections should adjust the RG flow of the gauge couplings so that the matching scale dependency is removed. Now in Fig. 4 we present an explicit demonstration of this effect in the E$_6$SSM with the threshold corrections we have calculated. The gauge couplings are plotted as a function of the renormalization scale for two different matching scales, $T_1 = 500$ GeV and $T_2 = 10$ TeV. If no threshold corrections are used (upper plot) different matching scales yield different predictions of M_X, which leads to a different phenomenology at the TeV scale. The inclusion of threshold corrections reduces this unphysical behavior. As shown in the lower plot, it leads to an approximately matching-scale independent prediction of M_X.

This improved behavior should manifest itself in a reduced scale dependence of model predictions at the TeV scale. As a test of this, Fig. 5 shows the E_6SSM gauge

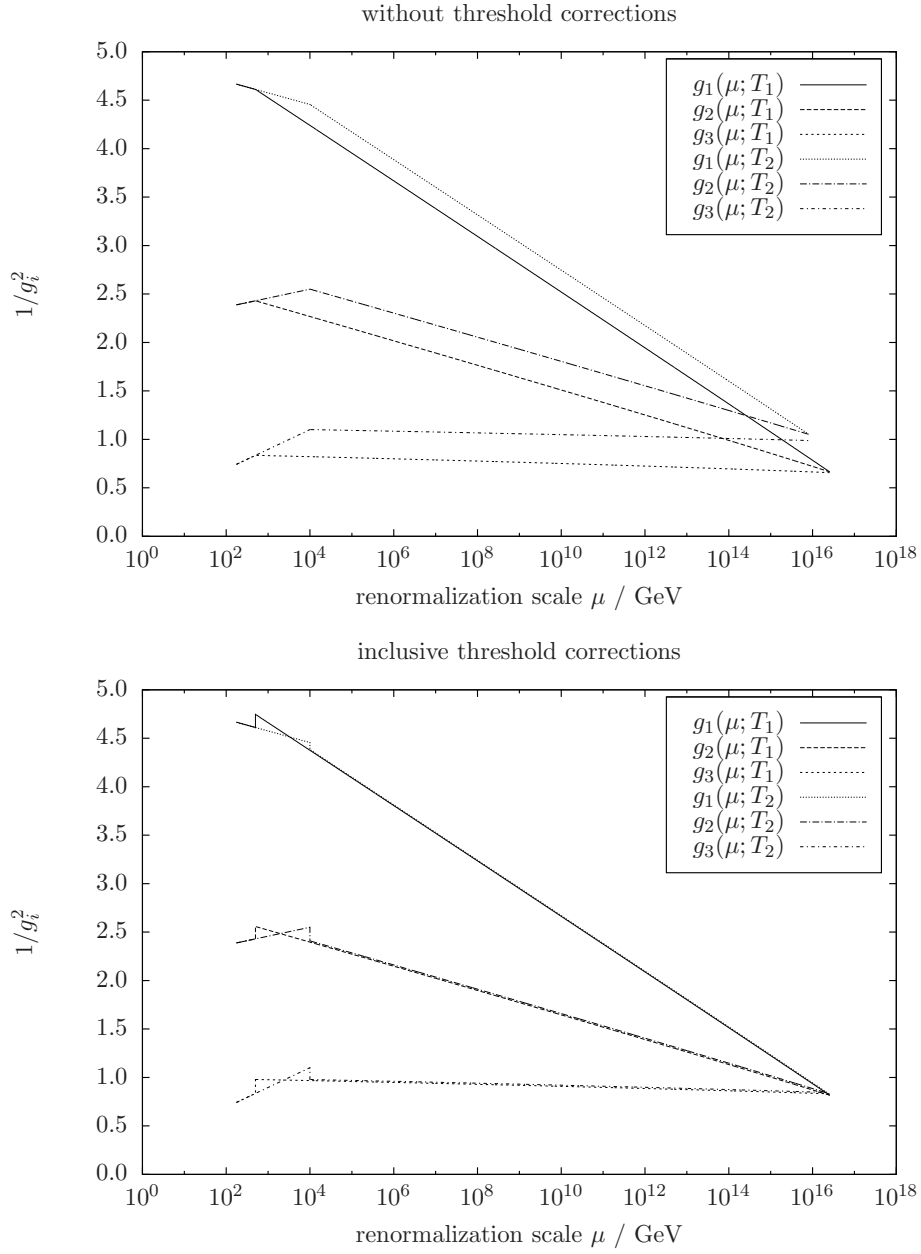

Fig. 4: Running gauge couplings for parameter point PP1 for two different matching scales $T_1 = 500$ GeV and $T_2 = 10$ TeV with and without threshold corrections.

couplings $g_i(Q_{\rm fix})$ at the fixed scale $Q_{\rm fix} = 3$ TeV, as a function of the matching scale $T_{\rm E_6SSM}$ for parameter point PP1. In the case of the trivial matching relations (59) one finds a clear (unphysical) dependence of $g_i(Q_{\rm fix})$ on $T_{\rm E_6SSM}$. As shown in Eq. (12) the slopes of $(4\pi)^2/[2g_i^2(Q_{\rm fix};T_{\rm E_6SSM})]$ are given by the difference $\Delta\beta_i := \beta_i^{\rm E_6SSM} - \beta_i^{\rm SM}$ of the one-loop gauge coupling beta functions, up to two-loop and iteration effects.

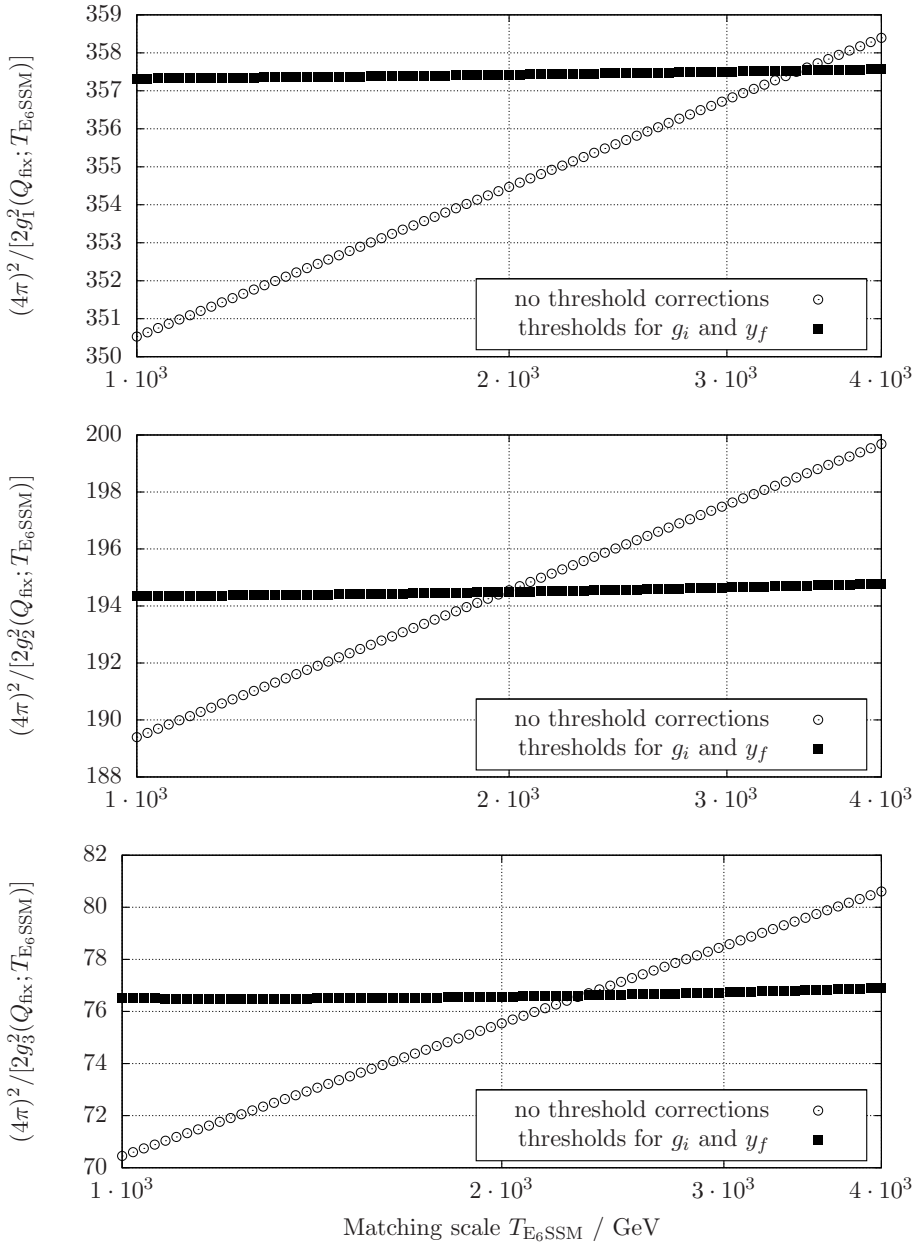

Fig. 5: Dependency of the gauge couplings g_i at $Q_{\rm fix} = 3$ TeV on the matching scale $T_{\rm E_6SSM}$ for parameter point PP1. The circles show the behavior without threshold corrections and the squares with corrections for g_i and y_f.

In Tab. 3, columns 4 and 5, the numerical values of $\Delta\beta_i$ as well as the slopes without threshold corrections for PP1 are listed. The values roughly coincide, thus confirming Eq. (12). When the threshold corrections (48), (49) and (32) are used, the matching scale dependency reduces to about 4 % or less, resulting in the flattening of the curves shown in Fig. 5. The remaining matching scale dependency as well as the difference between columns 4 and 5 are due to still missing contributions of higher orders.

Coupling	$\beta_i^{\mathrm{E_6SSM}}$	β_i^{SM}	$\Delta\beta_i$	slopes of $(4\pi)^2/[2g_i^2(Q_{\mathrm{fix}};T_{\mathrm{E_6SSM}})]$ w/o thresh.	w/ thresh.
g_1	9.6	4.1	5.5	5.67	0.18
g_2	4	−3.17	7.17	7.42	0.32
g_3	0	−7	7	7.33	0.29
	$\beta_f^{\mathrm{E_6SSM}}(T_{\mathrm{E_6SSM}})$	$\beta_f^{\mathrm{SM}}(T_{\mathrm{E_6SSM}})$	$-\Delta\beta_f$	slopes of $(4\pi)^2\log y_f(Q_{\mathrm{fix}};T_{\mathrm{E_6SSM}})$ w/o thresh.	w/ thresh.
y_t	−2.33	−6.14	−3.77	−3.81	0.77
y_b	−4.66	−8.18	−4.92	−4.95	−0.20
y_τ	−0.34	0.77	−0.29	−0.21	0.53

Tab. 3: Effect of the threshold corrections on the dependency of the gauge and Yukawa couplings on $T_{\mathrm{E_6SSM}}$ for parameter point PP1. The slopes in the last two columns are obtained by linear fits to the data in Fig. 5 and 6.

Fig. 6 shows the same analysis for the Yukawa couplings y_t, y_b and y_τ. Analogous to the gauge couplings one expects the following slopes of the Yukawa couplings as a function of the matching scale

$$\frac{\mathrm{d}\log y_t(Q_{\mathrm{fix}};t)}{\mathrm{d}t} = -\frac{1}{(4\pi)^2}\left[\beta_t^{\mathrm{E_6SSM}}(t) - \beta_t^{\mathrm{SM}}(t) + \beta_{\tan\beta}(t)\cos^2\beta\right] \equiv -\frac{1}{(4\pi)^2}\Delta\beta_t, \tag{65}$$

$$\frac{\mathrm{d}\log y_{b,\tau}(Q_{\mathrm{fix}};t)}{\mathrm{d}t} = -\frac{1}{(4\pi)^2}\left[\beta_{b,\tau}^{\mathrm{E_6SSM}}(t) - \beta_{b,\tau}^{\mathrm{SM}}(t) - \beta_{\tan\beta}(t)\sin^2\beta\right] \equiv -\frac{1}{(4\pi)^2}\Delta\beta_{b,\tau}. \tag{66}$$

Note that these relations also contain the β function for $\tan\beta$, defined in Eq. (D.14). In Tab. 3, columns 4 and 5, the numerical values of $\Delta\beta_f$ as well as the slopes without threshold corrections for PP1 are listed. One finds an agreement with the predicted slopes within a few percent. When the threshold corrections from Sec. 3.2 and 3.3 are taken into account one finds an overall reduction of the matching scale dependency effects. The remaining scale dependence is due to neglected higher-order effects, including in particular QED-logarithms of the small fermion masses in higher powers than taken into account in the one-loop computation of δm_f in Eqs. (50)–(52).

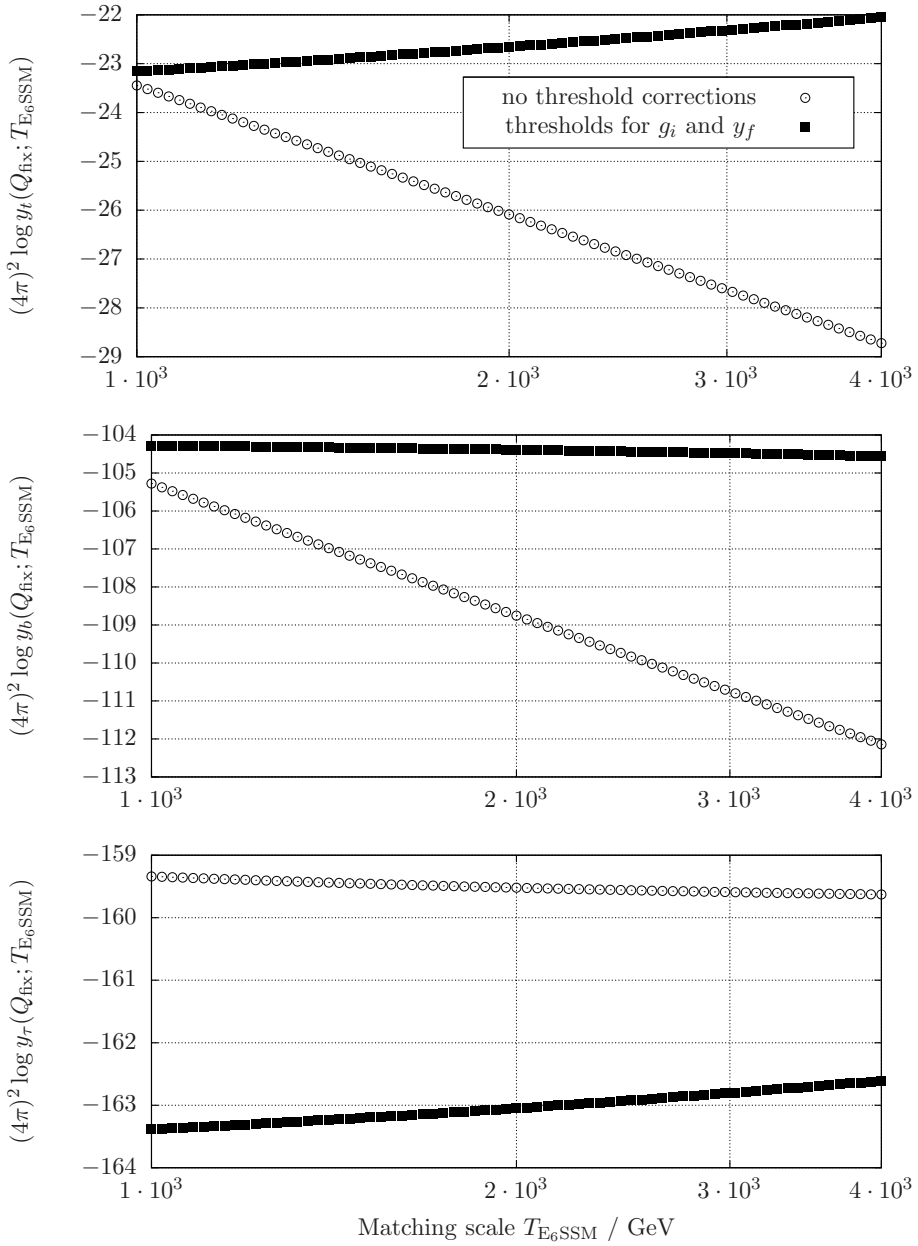

Fig. 6: Dependency of the Yukawa couplings y_f at $Q_{\rm fix} = 3\,\text{TeV}$ on the matching scale $T_{\rm E_6SSM}$ for parameter point PP1. The circles show the behavior without threshold corrections and the squares with corrections for g_i and y_f.

5.2 Particle masses

In softly broken SUSY models, like the CE$_6$SSM, where the pattern of soft breaking masses is set substantially above the EW scale (e.g. M_X), the low-energy $\overline{\rm DR}$ running masses are very sensitive to the renormalization group flow of the gauge and Yukawa couplings. This implies that the physical mass spectrum strongly depends on the matching scale used for the gauge and Yukawa couplings unless stabilized by the

inclusion of threshold corrections. Here we show how the inclusion of the CE$_6$SSM threshold corrections improves the prediction of the low-energy $\overline{\text{DR}}$ soft masses and yields a mass spectrum where the dependence on the unphysical matching scale is considerably reduced.

In Figs. 7 and 8 the dependency of the particle masses on the matching scale for parameter point PP1 is shown. The matching scale is varied in the range $[\frac{1}{2}T_0, 2T_0]$, where $T_0 = 1.9$ TeV is the geometric average of all particle masses shown in Fig. 8.

Fig. 7 focuses on the gluino. The theory uncertainty implied by the $T_{\text{E}_6\text{SSM}}$ dependence is 65 % without threshold corrections (the percentage value is defined as the full variation of the particle mass divided by the mass at T_0). This huge uncertainty is entirely due to the missing threshold corrections, and including these reduces the uncertainty to only 0.5 %.

Fig. 8 shows a subset of the generated particle spectrum for the parameter point PP1. The variation of the particle masses is drawn with a white box in case of trivial matching and with a black box in case of implemented threshold corrections. The gluino, the lightest chargino and the lightest neutralino show the biggest dependency with 65 %, 83 % and 85 %, respectively. With the implemented threshold

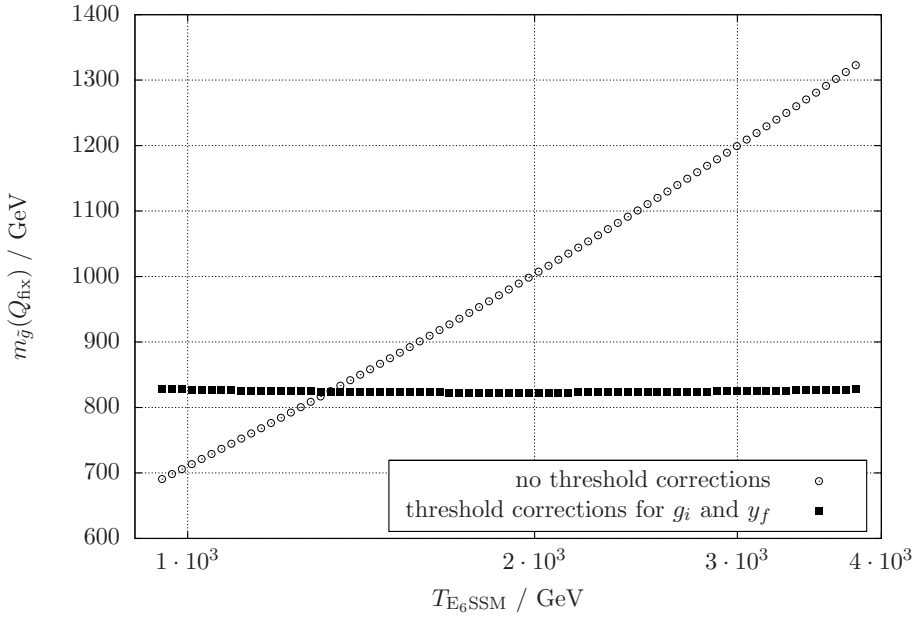

Fig. 7: Dependency of the gluino mass at $Q_{\text{fix}} = 3$ TeV on the matching scale $T_{\text{E}_6\text{SSM}}$ for parameter point PP1. The circles show the behavior without threshold corrections and the squares with corrections for g_i and y_f.

corrections, one finds a reduction of the variation down to 0.1–4 %. The biggest decrease is found for the gluino, the lightest chargino and the lightest neutralino

whose remaining variation is of the order of 0.5 %. This is because the gluino mass is very sensitive to g_3, as can be seen from the RGEs of the soft parameter M_3 [8]. Note that the remaining variation of the particle masses is due to 2-loop and iterative effects, which are of the order of up to 4 %.

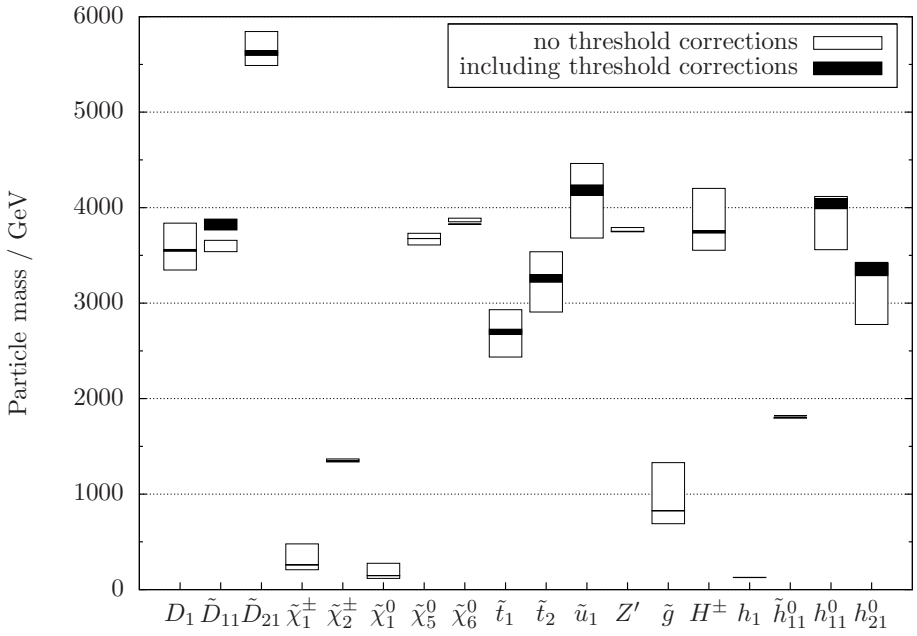

Fig. 8: Particle spectra for parameter point PP1. The white and the black boxes show the variation of the particle masses when the matching scale $T_{\mathrm{E_6SSM}}$ is varied in the interval $[\frac{1}{2}T_0, 2T_0]$, where $T_0 = 1.9$ TeV is the geometric average of all shown particle masses. The black boxes show the error with threshold corrections and the white boxes without.

Note that the variation of the matching scale is not always a good estimation of the theoretical uncertainty. For example the error band of $m_{\tilde{D}_{11}}$ without threshold corrections in Fig. 8 is shifted when adding threshold corrections but is not reduced in size. As can be seen in Fig. 9 the reason for the shift is the non-linear behavior of $m_{\tilde{D}_{11}}$ when $T_{\mathrm{E_6SSM}}$ is varied. In the interval $[\frac{1}{2}T_0, 2T_0]$ the exotic mass $m_{\tilde{D}_{11}}$ without threshold corrections happens to have a minimum which leads to an abnormally narrow error band. In contrast $m_{\tilde{D}_{21}}$ shows the typical, approximately linear behavior in $[\frac{1}{2}T_0, 2T_0]$ which leads to much better uncertainty estimation.

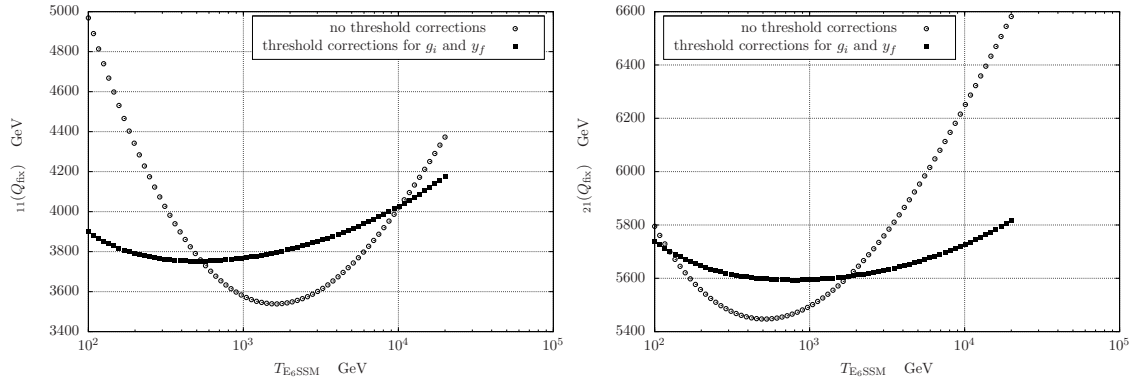

Fig. 9: Dependency of the first generation scalar exotic masses at $Q_{\rm fix} = 3$ TeV on the matching scale $T_{\rm E_6SSM}$ for parameter point PP1. The circles show the behavior without threshold corrections and the squares with corrections for g_i and y_f. In the interval $[\frac{1}{2}T_0, 2T_0]$ the exotic mass $m_{\tilde{D}_{11}}$ without threshold corrections has a minimum which leads to poor error estimation, whereas $m_{\tilde{D}_{21}}$ is approximately linear within this interval.

5.3 Exploration of the E$_6$SSM parameter space

5.3.1 Parameter space

We now turn from the specific benchmark point PP1 to a fuller investigation of the E$_6$SSM parameter space. Since our main focus is the impact of threshold corrections we still restrict ourselves to a two-dimensional slice of the 12-dimensional parameter space. We choose to keep the Yukawa couplings of the $SU(5)$ 5-plets containing $\hat{H}_{1i}$, $\hat{H}_{2i}$, $\hat{D}_i$ and $\hat{\bar{D}}_i$ the same and generation-independent, thus leaving a single unified exotic Yukawa coupling, defined at the GUT scale M_X,

$$\lambda_1 = \lambda_2 = \lambda_3 = \kappa_1 = \kappa_2 = \kappa_3 \tag{67}$$

between those states and the third generation singlet. In addition we fix

$$s = \mu' = m_{H'} = m_{\bar{H}'} = 10 \text{ TeV}, B\mu' = 0. \tag{68}$$

The remaining input parameters are $\tan\beta$ and λ_3, and we scan over them in the range

$$\tan\beta \in [2, 45], \qquad \lambda_3 \in [0, 3]. \tag{69}$$

Note that we are defining λ_3 at the GUT scale, and in this respect the numerical value should not be compared with λ in the NMSSM which is often defined near the

electroweak scale (EW). By defining λ_3 at the GUT scale we ensure automatically that it is perturbative at all scales between the electroweak and the GUT scale.[6]

For each choice of $(\tan\beta, \lambda_3)$, requiring electroweak symmetry breaking simultaneously with (68) leads to up to four solutions for $(m_0, M_{1/2})$, which we number consecutively. In the following $(m_0, M_{1/2})$-plots we will show all of them, where solution 1 is preferred over solution 2 in the overlap region. In Figs. 18–19 we will show only the first solution for simplicity.

Since our input parameters $(\tan\beta, \lambda_3)$ have less direct physical meaning than the output parameters $(m_0, M_{1/2})$, we display many results in the $(m_0, M_{1/2})$ plane. To better understand the connection between these two sets we show in Fig. 10 the mapping of $(\tan\beta, \lambda_3) \to (m_0, M_{1/2})$. In the top panel we show as a color contour plot how $\tan\beta$ varies over the $(m_0, M_{1/2})$ plane, while on the lower plot we do the same for λ_3. Fig. 10 thus allows to read off the original input values for $(\tan\beta, \lambda_3)$ for any given point in the subsequent plots.

The butterfly shape of Fig. 10 is due to the superposition of the four solutions. Most of the $(m_0, M_{1/2})$ space is covered by relatively small $\lambda_3 < 0.4$, while larger values of lambda are concentrated in a narrow region of the parameter space due to the renormalisation group flow leading to a focusing on a significantly smaller range of λ_3 at the electroweak scale. The $\tan\beta$ dependency depends on the solution, but in much of the parameter space large values of $\tan\beta$ are associated with large m_0 and small $M_{1/2}$.

Fig. 10 is not exactly symmetric in $\pm M_{1/2}$ because λ_3 and therefore the effective μ-parameter is required to be positive in our analysis.

5.3.2 Experimental constraints

At this point we briefly summarize the various experimental constraints on the model. A more detailed discussion can be found in [10].

Since the publication of the first studies of the CE_6SSM [8, 9] the Atlas and CMS experiments have already placed strong constraints on supersymmetry from the first $\approx 5\ \text{fb}^{-1}$ of data gathered from the LHC running at $\sqrt{s} = 7$ TeV. With $4.7\ \text{fb}^{-1}$ of data Atlas have performed searches for squarks and gluinos, by looking for jets plus missing transverse momentum and possibly one isolated lepton [43, 44, 45] and

[6] In the NMSSM it is well known that to ensure perturbativity $\lambda(\text{EW}) \lesssim 0.7$, while an analysis of this in the E_6SSM [2] found that $\lambda_3(\text{EW}) \lesssim 0.85$ is required for perurbativity up to the GUT scale, though this limit depends on the values of the other exotic Yukawa couplings and $\tan\beta$.

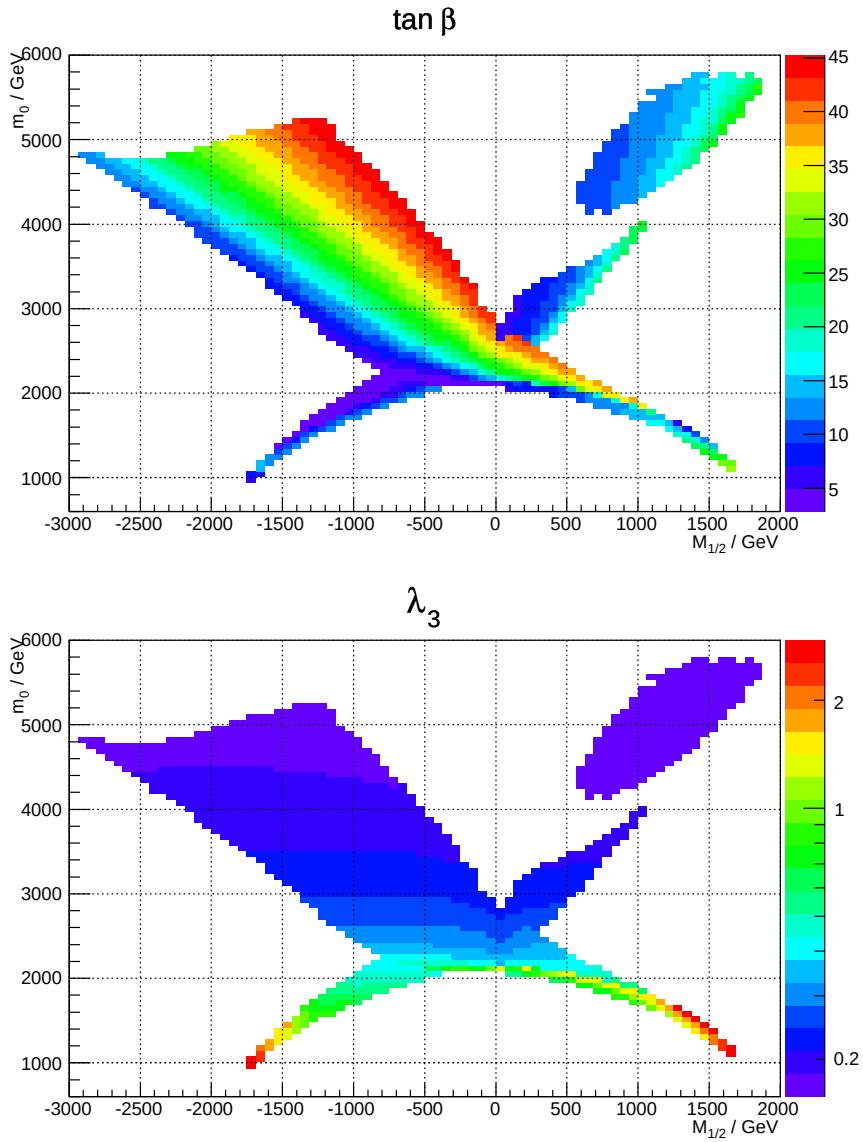

Fig. 10: Illustration of the mapping $(\tan\beta, \lambda_3) \to (m_0, M_{1/2})$. The top panel shows the input parameter $\tan\beta$ varying across the $(m_0, M_{1/2})$ plane (of output parameters). The bottom panel shows the same for the input parameter λ_3.

presented the constraints in a CMSSM interpretation.[7] CMS collaboration have also placed similar constraints using the razor analysis [46] with 4.4 fb^{-1} of data [47] and another analysis with the transverse mass variable [48] using 4.73 fb^{-1} of data. Very recently the ATLAS released updated results with 5.8 fb^{-1} data from the $\sqrt{s} = 8$ TeV run [49].

[7]They also presented constraints in a simplified model interpretation, however this is less relevant for our present purposes since the physical spectrum of our model, especially if the colored exotics are heavy, is far closer to that of the CMSSM than the simplified models.

It was estimated in [50, 10] that the effect of these constraints on the CE_6SSM is to place a limit on the gluino mass, close to 850 GeV. Since the squarks must always be heavier than the gluino, due to the RG flow,[8] squark limits are automatically satisfied. However the 8 TeV data has increased the limits on the gluino, in the heavy squarks region the limit varies between $\approx$ 900–1000 GeV.

However it is also of interest to point out that in certain E_6SSM scenarios (where the bino-like neutralino is not stable, leading to longer cascade decays and an alternative LSP) the gluino limits from these searches may not apply [18] resulting in different limits.

Furthermore, there are limits on the Higgs mass [51, 52] from analyses using between 4.6 and 4.9 fb^{-1} of LHC data. At 95 % confidence level Atlas exclude a standard model Higgs in the ranges 110.0–117.5 GeV, 118.5–122.5 GeV and 129–539 GeV, while at the same confidence level CMS exclude 127.5–600 GeV. This leaves a narrow allowed window of 117.5–118.5 GeV and a wider one of 123.5–127.5 GeV.

As this paper was being finalized the discovery of a new particle consistent with a Higgs boson with a mass of around 125–126 GeV was announced by ATLAS [28] and CMS [29]. CMS report a 5.0σ excess at 125.5 GeV and quote a best fit mass of $125.3 \pm 0.4(\text{stat.}) \pm 0.5(\text{syst.})$ GeV while ATLAS find a 6.0σ excess at 126.5, and using the two channels with the highest mass resolution estimate the mass as $126.0 \pm 0.4(\text{stat.}) \pm 0.4(\text{syst.})$ GeV.

The strongest current constraint on the Z'_N comes from a CMS analysis using ≈ 5 fb^{-1} of data [53], announced as this paper is being finalized and setting a lower limit of 2.08 TeV on the mass of the Z'_N boson. However one should note that the lower limit assumes there are now light exotics available for the Z' to decay into. If such are present then the branching ratio to leptons is diluted and the limits are weaker.

Finally the model also contains exotic (colored and inert) fermions and sfermions. The inert states are weakly produced and we do not anticipate very large new limits to be set by the early data from the LHC, but the colored states should be produced abundantly and could be tightly constrained. However the existing analyses do not apply to the fermionic diquarks or leptoquarks described in this model since they carry half integer spin and are odd under their respective discrete symmetries, decaying with missing energy. Thus it is currently unknown what limit the LHC

[8] The soft scalar masses get large contributions (relative to the gauginos) from $M_{1/2}$, due to the renormalization group evolution, which is very different from the MSSM case.

has placed on their mass. Here we will only consider cases where these exotics are heavy anyway but when discussing existing benchmarks from the literature we will not apply any new constraints on them.

The E_6SSM also contains a number of dark matter candidates. It is possible that the correct relic density can be achieved entirely from the inert sector neutralinos (admixtures of inert singlinos and inert higgsinos) [54] however such a scenario is now in conflict with XENON-100 limits [55] though if one allows for a relic density which is too small to explain observations (and therefore would require some additional contributions to dark matter) consistency could be achieved. Alternatively another possible scenario described in Ref. [56] is that there is a large splitting between the inert states with one at a few keV and another a few GeV, thus giving warm dark matter scenarios, which match observation. For cases studied the couplings which are assumed to be negligible here are too large to avoid perturbing the RG evolution and may be too large for consistency with the constrained model generally. However such scenarios have only recently been proposed and the full parameters space far from explored so it is simply unknown whether or not this could be applied with couplings which would be consistent with the scenarios explored here.

A third possibility which is known to be consistent with the constrained version of the model decouples the singlinos from the rest of the spectrum, giving a new contribution to the effective number of neutrinos (which is consistent with observation) [57]. The bino is then the dark matter candidate, but the scenario is still very distinct from typical models with bino dominated dark matter because the inert Higgsinos play a crucial role in enabling the correct relic density to be achieved so long as the mass of the lightest inert neutralino is related to that of the lightest neutralino by the condition [57],

$$\mu_{\tilde{H}_1} \approx |m_{\tilde{\chi}_1^0}| + 10 \text{ GeV}. \tag{70}$$

In the scans we perform here we do not explicitly satisfy this constraint (and instead our inert Higgsinos are typically far heavier) as we assume a universality amongst all exotic Yukawa couplings. Splitting one generation of all exotics or just inerts could solve this problem. Doing so would perturb the renormalization group equations and distort the parameter space somewhat, though the qualitative results and understanding of the impact that these thresholds can have would not be altered. Alternatively one can keep in mind the "keVins and GeVins" scenarios though it is currently unknown if this could result in the correct relic density or not.

5.3.3 Change in masses from threshold corrections

Now we look at the significance of the threshold effects throughout the parameter space described in Sec. 5.3.1. Like for the point PP1, the largest corrections are observed in the gaugino sector for states whose masses are set by $M_{1/2}$. Fig. 11 shows the shifts in mass for the gluino and lightest neutralino in the $(m_0, M_{1/2})$-plane.[9] We compare between results with trivial matching conditions to those with full threshold corrections, where in both cases the matching scale used is the "optimal" choice, where $T_{\mathrm{E_6SSM}}$ is set to the geometric average of the particle masses.

We show the absolute change in masses rather than relative change because, when the masses are light due to a cancellation, the relative corrections can be very large, distorting the plot. However it is important to note that the gaugino masses though not shown can be estimated since the low-energy soft gaugino masses M_i (which give the dominant contribution to $m_{\tilde{g}}$ and $m_{\tilde{\chi}_1^0}$) are proportional $M_{1/2}$, with $m_{\tilde{g}} \sim 0.85 M_{1/2}$, $m_{\tilde{\chi}_1^0} \sim 0.15 M_{1/2}$. Fig. 12 shows the actual gluino and neutralino masses after including threshold corrections for comparison.

Once again we see substantial changes in both the gluino and neutralino mass across a wide range of the parameter space with corrections being small only in a very narrow region of the space. Around the LHC limit on gluinos we can see there can be large corrections of the order of several 100 GeV for the gluino mass, therefore these corrections can make a significant impact in determining whether or not a point is ruled out by LHC search constraints. The corrections to the gluino mass can be positive or negative, depending on whether the masses appearing in the logarithmic corrections are larger or smaller than the threshold scale.[10]

The corrections to the neutralino are also substantial, varying from just below zero to just over 200 GeV. They are distinctly correlated with the corrections to the gluino, showing close to identical variation, which is because the dominant effect is a shift in $M_{1/2}$.

With the recent discovery of a Higgs-like boson [28, 29] with a mass $\approx$ 125–126 GeV and strong constraints on a SM-like Higgs away from the mass of this new state, the lightest Higgs mass is a crucial observable in constraining the parameter space of SUSY models. The corrections to the lightest Higgs mass from threshold effects are not expected to be very large since it's mass is not set by soft mass parameters

[9] Note that these are the m_0 and $M_{1/2}$ values obtained from the spectrum generator when thresholds are included. Since m_0 and $M_{1/2}$ are outputs they are affected by the threshold corrections and so do not match the values for the point without threshold corrections.

[10] In this case the dominant corrections arise from corrections to g_3, see Eq. (32).

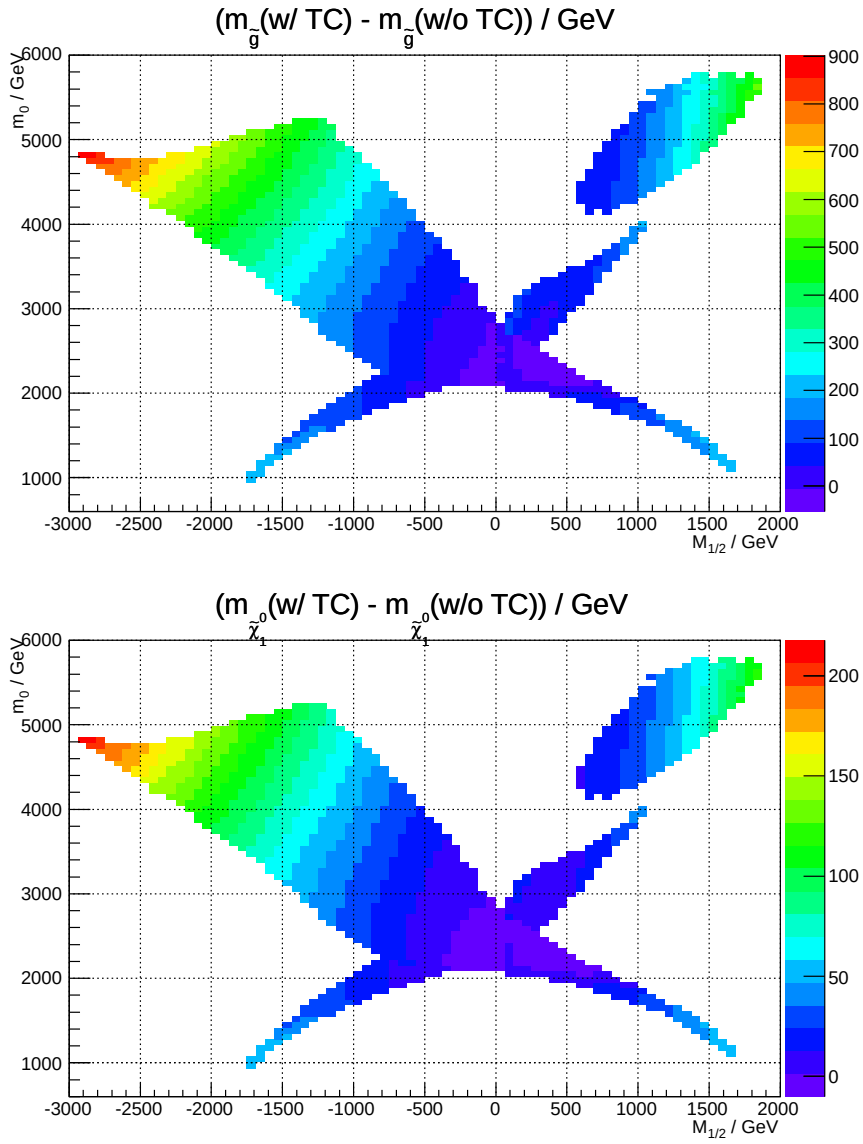

Fig. 11: Change in the gluino and in the lightest neutralino mass when adding threshold corrections for $s = \mu' = m_{H'} = m_{\bar{H}'} = 10$ TeV, $\tan\beta \in [2, 45]$ and $\lambda_i(M_X) = \kappa_i(M_X) \in [0, 3]$.

at tree level. However even small corrections to the Higgs mass can significantly shift the m_0 and $M_{1/2}$ values which a particular Higgs mass is compatible with and this can dramatically alter how the Higgs mass measurement combines with the constraints coming from squark and gluino searches.

In Fig. 13 the corrections to the Higgs mass are shown across the $(m_0, M_{1/2})$-plane. The corrections vary between around -0.7 GeV to $+1.7$ GeV. One can also see in Fig. 14 the Higgs mass itself and note that for the parameter set studied here the Higgs mass is consistent with the new particle discovered by ATLAS and CMS

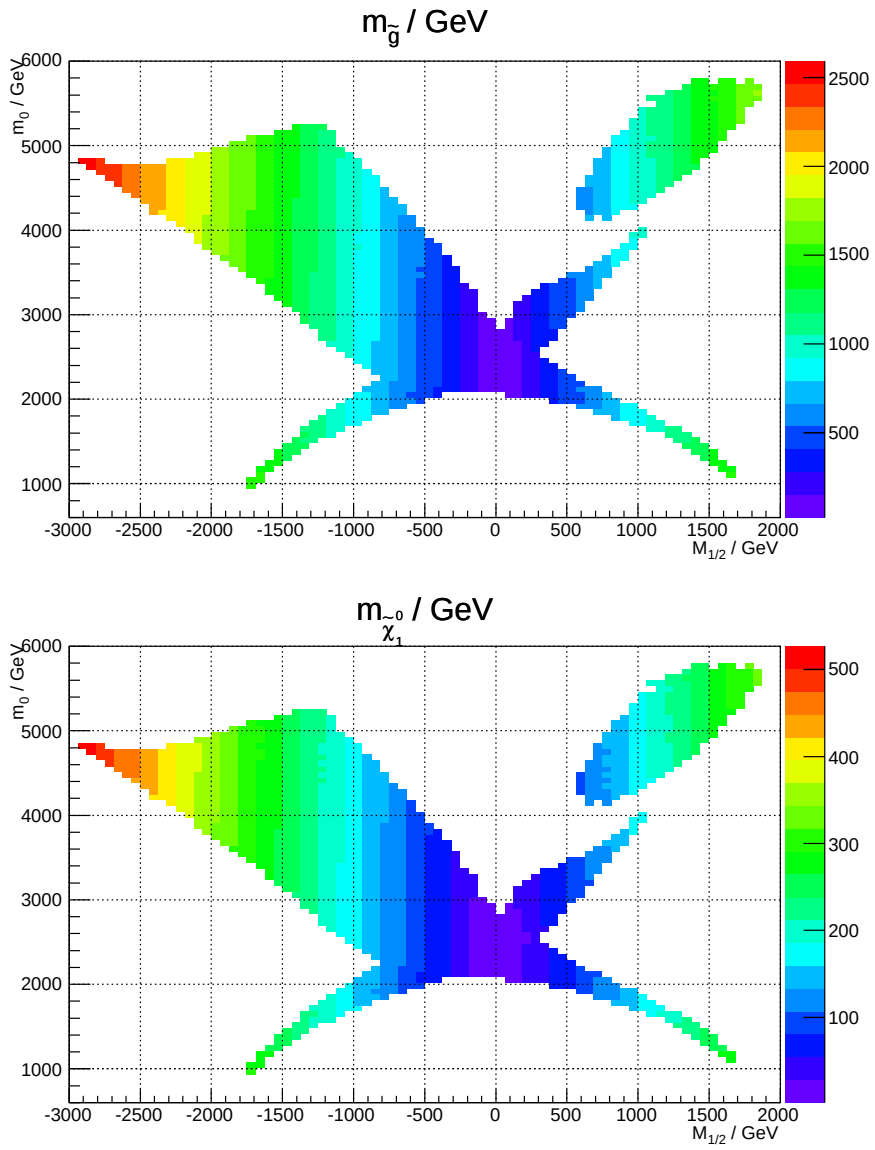

Fig. 12: Gluino and in the lightest neutralino mass as a function of $M_{1/2}$ and m_0, where it was varied $\tan\beta \in [3, 50]$, $\lambda_i = \kappa_i \in [0, 3]$, $s = 10$ TeV, $\mu' = m_{H'} = m_{\bar{H}'} = 10$ TeV.

in the large m_0 and $M_{1/2}$ regions of the parameter space where the corrections from the thresholds are largest.

5.3.4 Allowed parameter space

With the more reliable predictions at hand, we turn to understanding the overall allowed region of parameter space. Dominant experimental constraints come from the gluino and the Higgs, see Figs. 12 and 14. We can see that for our choice of s the gluino is comfortably above the LHC limit in a large volume the parameter space.

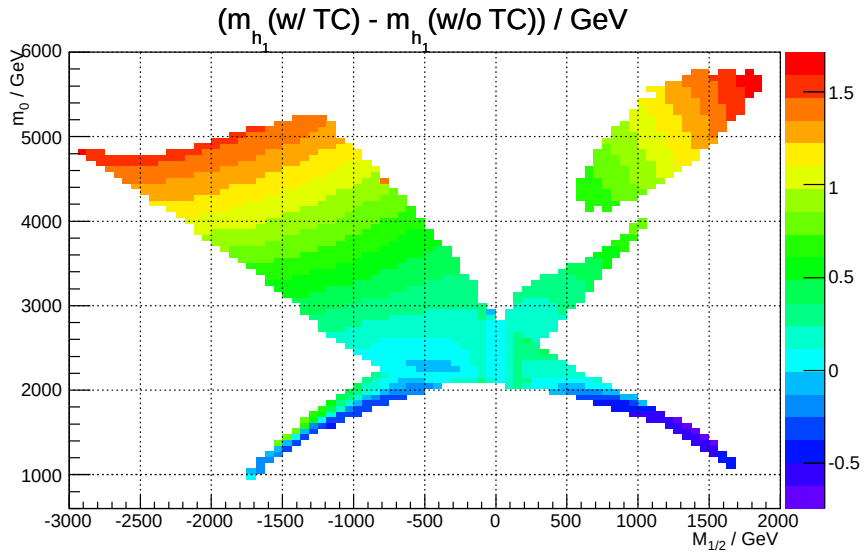

Fig. 13: Change in the lightest CP even Higgs mass when adding threshold corrections for $s = \mu' = m_{H'} = m_{\bar{H}'} = 10$ TeV, $\tan\beta \in [2, 45]$ and $\lambda_i(M_X) = \kappa_i(M_X) \in [0, 3]$. We show only points where the change is less than 5 GeV.

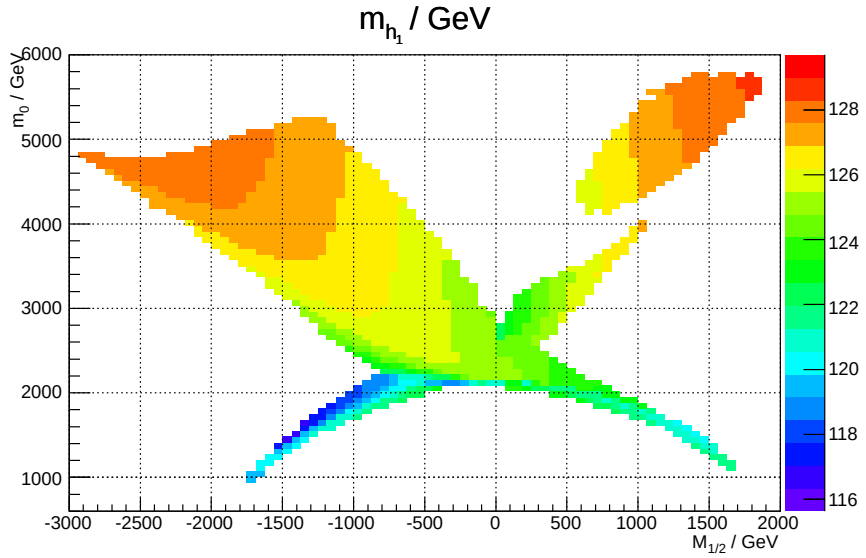

Fig. 14: Lightest CP even Higgs mass m_{h_1} as a function of $M_{1/2}$ and m_0, where it was varied $\tan\beta \in [3, 50]$, $\lambda_i = \kappa_i \in [0, 3]$, $s = 10$ TeV, $\mu' = m_{H'} = m_{\bar{H}'} = 10$ TeV.

In the Higgs contour plot Fig. 14 we also see a very large volume of the parameter space where the light Higgs mass is within the narrow window on it's allowed mass from the LHC discovery. Nevertheless in fact the combination of the two constraints creates very stringent limits of this slice of the parameter space.

To show the impact more precisely we now plot in Fig. 15 the valid and invalid parameter space including all relevant constraints, both in terms of $(\tan\beta, \lambda_3)$ and of $(m_0, M_{1/2})$. While it is beyond the scope of the current project to take account of full experimental likelihoods or include precise 95% confidence limit contours, to provide a guide as to the parameter space which evades LHC constraints we define valid points as those satisfying,

$$123.5 \text{ GeV} < m_{h_1} < 127.5 \text{ GeV}, \tag{71}$$

$$m_{\tilde{g}} > 1 \text{ TeV}, \tag{72}$$

$$m_{\tilde{t}_1} > 300 \text{ GeV}, \tag{73}$$

$$m_{\tilde{\chi}_1^0}, m_{\tilde{\chi}_1^\pm} > 200 \text{ GeV}, \tag{74}$$

$$m_{Z'} > 2.1 \text{ TeV}, \tag{75}$$

$$m_{\tilde{h}_{li}^0}, m_{\tilde{h}_i^+}, m_{h_{ij}^0}, m_{h_{ij}^\pm} > 100 \text{ GeV}, \tag{76}$$

which are based on the discussion of Sec. 5.3.2.

One finds that the lower bound on $m_{\tilde{g}}$ and the bounds on m_{h_1} are most constraining. This is because the gluino is driven lighter than the sfermions by the renormalization group flow with, $M_3 \sim 0.7 M_{1/2} \sim$ 200–1400 GeV, while for the Higgs we now have a very narrow range of allowed masses as a result of Higgs searches that ultimately lead to the recent discovery. Here we find the lightest Higgs mass is around $m_{h_1} \sim$ 118–128 GeV [8], as shown in Fig. 14, including a substantial region of parameter space where the CE$_6$SSM predicts a lightest Higgs with a mass of 123.5–127.5 GeV, consistent with the discovery.

While the allowed region appears strongly restricted in $(\tan\beta, \lambda_3)$-space, it appears reasonably large in the $(m_0, M_{1/2})$-plane. The reason is the non-trivial mapping between these two spaces, as illustrated by Fig. 10. The valid green region in the $(\tan\beta, \lambda_3)$-space of Fig. 15 is mapped onto different wings of the butterfly in the $(m_0, M_{1/2})$-plane.

Fig. 15 also shows that even without imposing experimental constraints there are upper and lower limits on all the parameters. Outside the colored regions no simultaneous solution to electroweak symmetry breaking and unification without tachyonic masses can be found. In particular, there is an upper limit on $\tan\beta$ at around 45. Here the EWSB minima become unstable giving a tachyonic Higgs mass, as shown in Fig. 16 for both the uncorrected Higgs mass and for the threshold corrected value, which converge in this region. At such large $\tan\beta$ the bottom quark Yukawa coupling is much closer to the top quark Yukawa coupling, and in such a

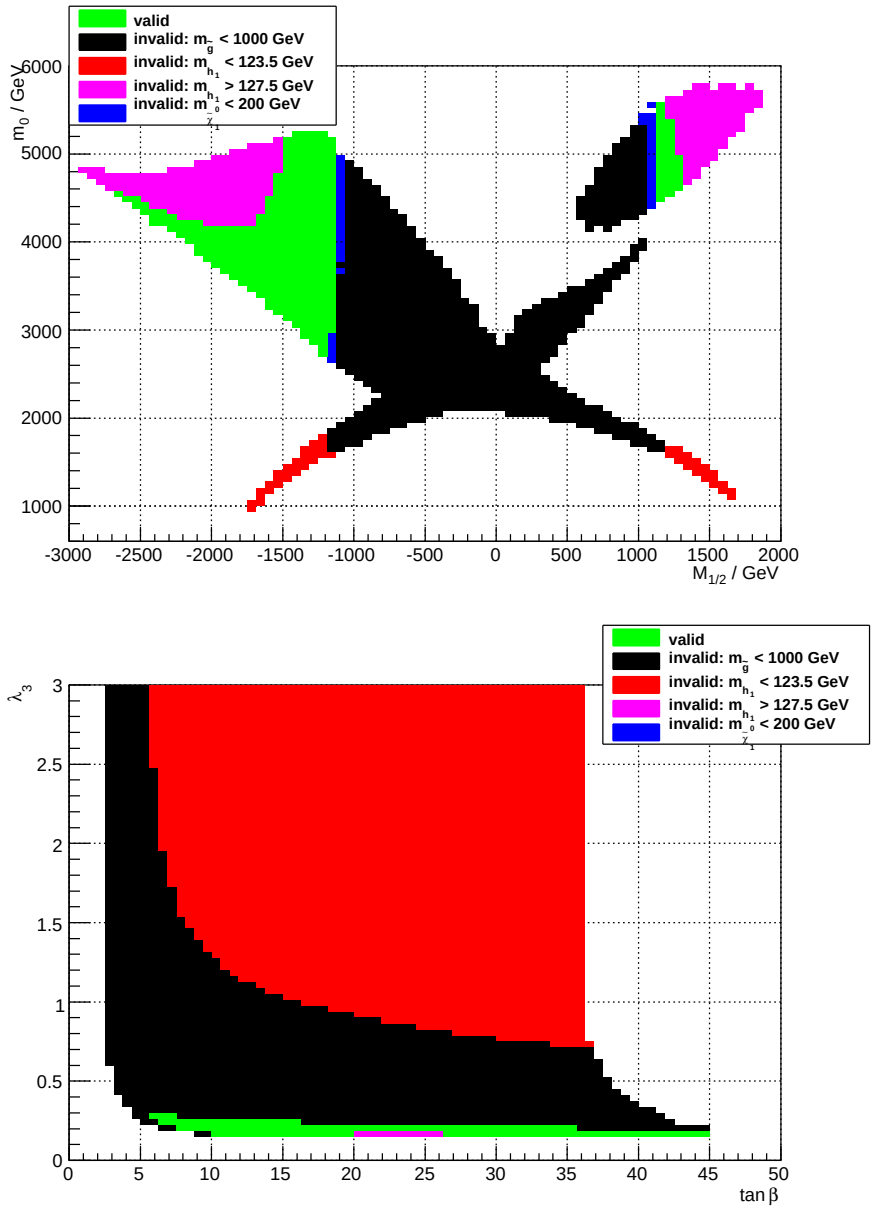

Fig. 15: Exclusion plot of the E_6SSM parameter space.

situation generating a large splitting between the Higgs masses required for correct EWSB is difficult. A simple tree-level condition for keeping $m_A^2 > 0$ at large $\tan\beta$ can be derived in the MSSM [58] and in the E_6SSM,

$$\text{MSSM: } m_{H_d}^2 - m_{H_u}^2 \gtrsim m_Z^2, \tag{77}$$

$$\text{E}_6\text{SSM: } m_{H_d}^2 - m_{H_u}^2 \gtrsim m_Z^2 + \frac{g_N^2}{4}\Sigma_Q(N_{H_2} - N_{H_1}). \tag{78}$$

The E_6SSM condition is stricter since it contains an additional positive term involv-

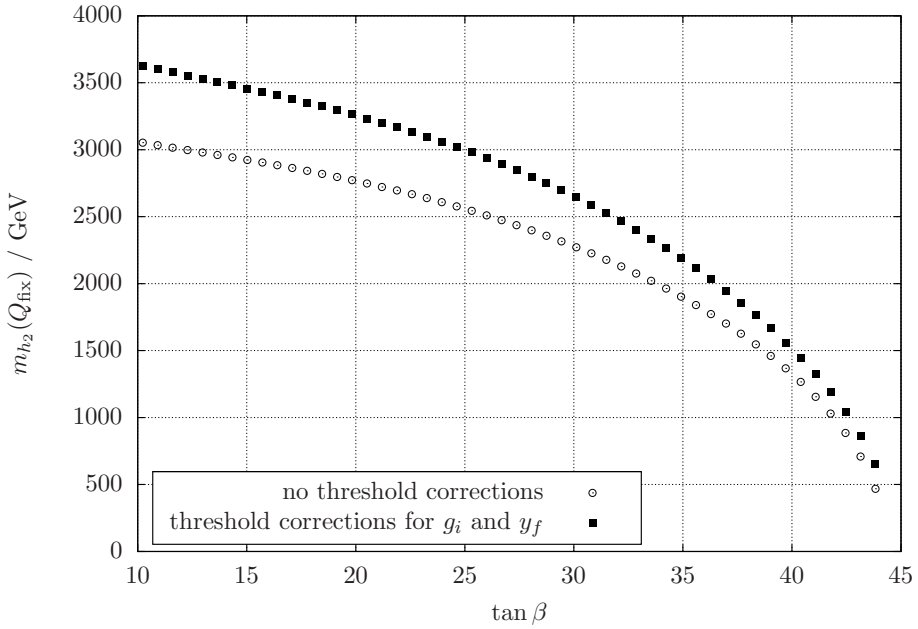

Fig. 16: Second lightest CP even Higgs mass as a function of $\tan\beta$ for $s = \mu' = m_{H'} = m_{\bar{H}'} = 10$ TeV and $\lambda_i(M_X) = \kappa_i(M_X) = 0.2$

ing,[11]

$$\Sigma_Q = \frac{1}{2}(N_{H_1} v_1^2 + N_{H_2} v_2^2 + N_S s^2). \tag{79}$$

5.4 Dependency on the survival Higgs parameters

The inclusion of threshold corrections not only reduces the unphysical matching-scale dependence. It also leads to a physical dependence on the survival Higgs sector. Without thresholds the spectrum does not explicitly depend on the survival Higgs masses as the renormalization group equations decouple. With threshold corrections the survival Higgs parameters appear in the threshold corrections to the gauge couplings, and thus affect both gauge coupling unification and the low-energy mass spectrum. We will now study these two aspects in a simplified setting by taking a single scale

$$m_{\rm surv} \equiv \mu' = m_{H'} = m_{\bar{H}'}. \tag{80}$$

Figs. 17 and 18 focus on gauge-coupling unification. We recall that in our approach M_X is defined by the intersection of g_1 and g_2, while g_3 is determined by its running from its low-energy measured value. Fig. 17 shows that for the parameter choice PP1, exact unification can be achieved by adjusting $m_{\rm surv} = 200$ GeV, while

[11] The term is positive so long as $s > v$, which is always the case due to limits on the Z' mass.

e.g. $m_{\rm surv} = 16$ TeV leads to a substantial deviation between g_3 and g_2 at the GUT scale.

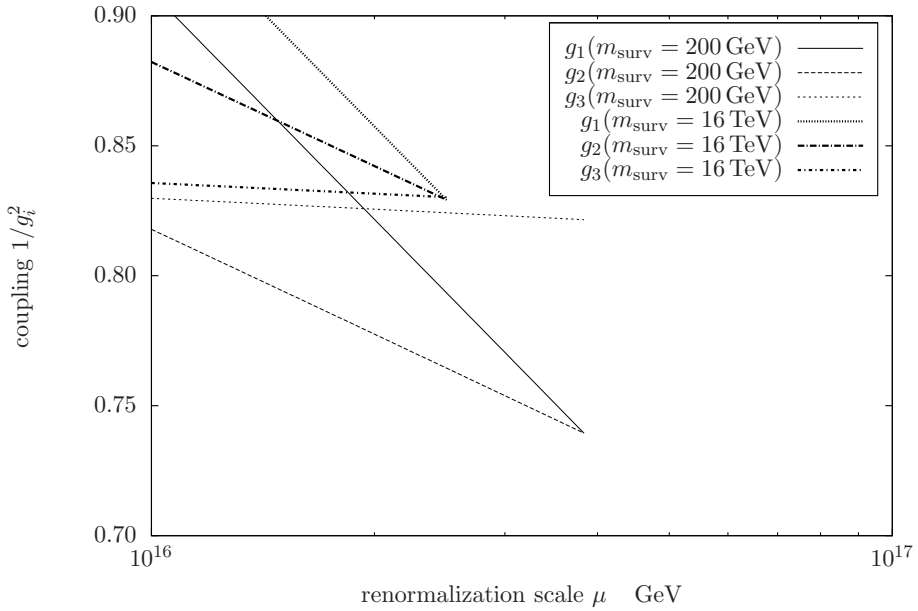

Fig. 17: Splitting between g_1 and g_3 at M_X for two different choices of $m_{\rm surv}$ for PP1.

Of course in a full GUT model there will be GUT scale threshold corrections. Nevertheless Fig. 17 makes clear that requiring a precise splitting between the gauge couplings from any given GUT threshold correction will fix the survival Higgs scale.

Fig. 18 shows gauge coupling (non-)unification for the entire parameter space defined by Eqs. (67)–(69) except that $\tan\beta = 10$ is fixed and $m_{\rm surv}$ is varied in the range

$$m_{\rm surv} \in [0.1, 1000]\ {\rm TeV}. \tag{81}$$

Like in Fig. 17, we find that the deviation $(g_1 - g_3)$ at M_X depends substantially on the survival Higgs masses, and for any given lambda there is a survival Higgs scale which allows exact unification or any splitting required by GUT thresholds between 0 and $O(0.1)$.

Figs. 19 and 20 focus on the influence of $m_{\rm surv}$ on the mass spectrum. In Fig. 19 we plot the variation of the gluino mass across the $(m_{\rm surv}, \lambda_3)$-plane and see that the dependence on the survival Higgs masses is extremely weak. The figure also shows that the lightest neutralino mass is affected slightly more, in particular in regions where it is rather heavy ($\sim$ 250–300 GeV).

Typically the survival Higgses and Higgsinos are too heavy to be observed at

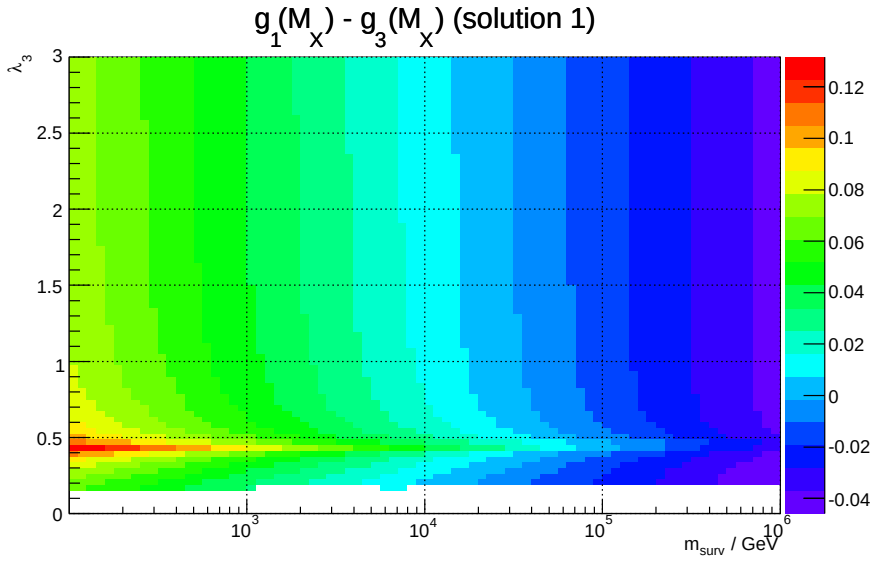

Fig. 18: Splitting between g_1 and g_3 at M_X in the $(\lambda_3, m_{\rm surv})$ parameter space

the LHC, since they are only weakly produced and have the couplings of a 4th generation lepton with current mass limit on the mass of 100.8 GeV.

For cases where they are not observable and where we do not constrain the splitting between the gauge couplings at the GUT scale, we can therefore consider them as an additional error in the theoretical calculation. This is the approach we now take here. To look at this in detail we again turn to our test case PP1.

Fig. 20 shows the dependency of the particle spectrum on the new model parameter $m_{\rm surv}$ for PP1. It is instructive to compare the result to Fig. 8, where the sensitivity to the matching scale $T_{\rm E_6SSM}$ with and without threshold corrections is shown. In the comparison one has to bear in mind that the $m_{\rm surv}$-dependence is physical and that we vary $m_{\rm surv}$ in a much larger interval than $T_{\rm E_6SSM}$.

One finds a significant $m_{\rm surv}$-dependence only for masses which were also strongly sensitive to the choice of matching scale without threshold corrections. This is because a variation of $T_{\rm E_6SSM}$ changes the size of all the logarithmic contributions to the threshold corrections, while the variation of $m_{\rm surv}$ changes a subset of contributions to the thresholds. However, we also find that after including threshold corrections the $m_{\rm surv}$-dependence is generally larger than the remaining matching-scale dependency.

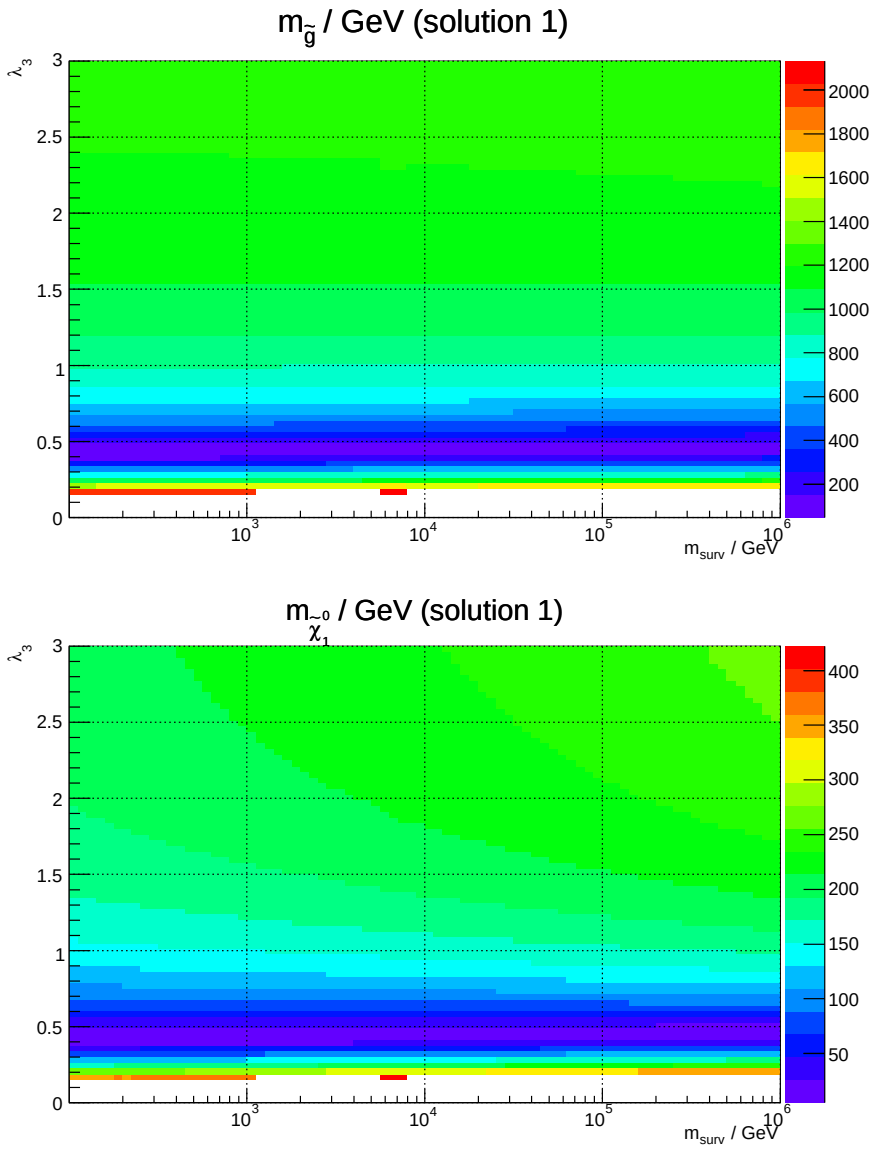

Fig. 19: Gluino mass $m_{\tilde{g}}$ and mass of the lightest neutralino $m_{\tilde{\chi}_1^0}$ in the $(\lambda_3, m_{\rm surv})$ parameter space

5.5 Benchmarks in the literature

As a final application of the threshold corrections presented here we now study the impact they have on previously published benchmarks in the model which have appeared in [8, 9, 10]. The 1 TeV limit for the gluino which we require to be consistent with Atlas and CMS searches is above the masses of the all light benchmarks [8, 9], while heavy benchmarks [10] were chosen to be safe from these limits. However since the threshold effects presented here have a very large impact on the gluino mass, clearly they play an important role in determining whether or not a particular $\mathrm{CE_6SSM}$ point is excluded. We will therefore study what impact the threshold ef-

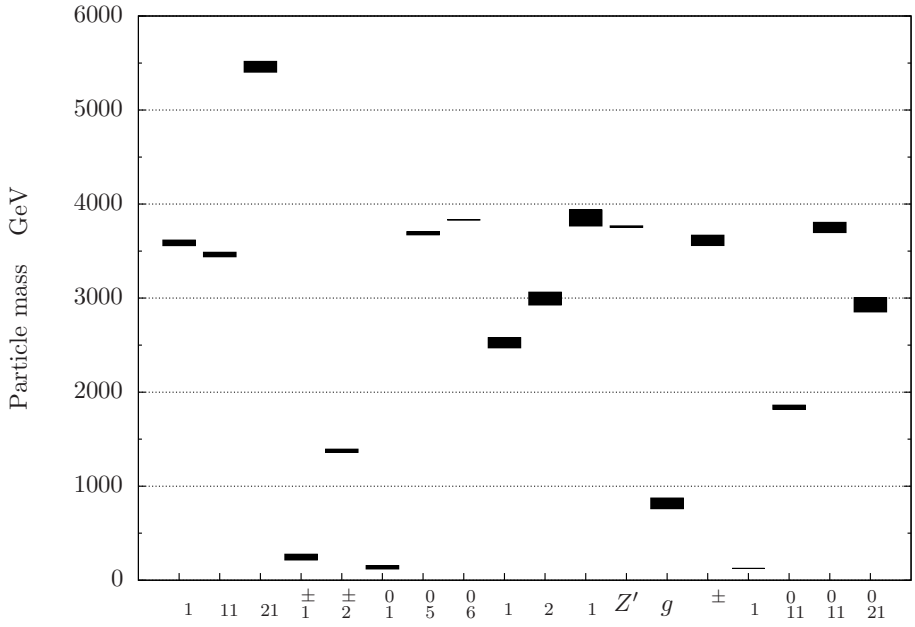

Fig. 20: Dependence of the particle spectrum on the survival Higgs scale $m_{\rm surv} = 0.1$–10 TeV for parameter point PP1.

fects have on all these points and in particular whether it changes their experimental status.[12]

The benchmarks in Refs. [8, 9] were selected to have very light gauginos or be close to the lower limit on m_0 (for that choice of singlet VEV s), where one can get lighter exotic sfermions. Below this lower limit on m_0 the inert Higgs scalars become tachyonic due to the large $U(1)_N$ D-terms which give a negative contribution to the mass.

As a result of this the threshold corrections can push some points into the region with tachyonic masses. Since we are applying the threshold corrections iteratively this creates a problem. It may be that such points in fact do not contain tachyonic solutions but merely the first step in the iteration jumps to that region and subsequent steps, if they could be performed, would lead to a self consistent tachyon free solution. In this case we try pushing the point into a convergent iteration by adjusting the thresholds corrections in the early steps. If this does not work we then vary the survival Higgs mass to see if this can lead to tachyon free solutions.

The impact on the gluino mass of these threshold corrections, for all the points

[12]All but one of the light benchmarks have a Z' mass substantially below the limit discussed in Sec. 5.3.2. Light exotics, like singlinos, which are necessarily present in the E$_6$SSM, will give a substantial reduction in the limit. This is probably not sufficient to evade the limits, but nonetheless testing against constraints from gluino searches provides another important limitation on the viability of these scenarios.

$m_{\tilde{g}}$ / GeV	BMA	BMB	BMC	BMD	BME	
without thresholds	336	330	353	327	338	
including thresholds	224	269[b]	260	230	203[b]	
$m_{\tilde{g}}$ / GeV	BM1	BM2	BM3	BM4	BM5	BM6
without thresholds	350	673	362	642	338	805
including thresholds	322	613[a]	275	423[a]	190	825
$m_{\tilde{g}}$ / GeV	HBM1	HBM2	HBM3	HBM4	HBM5	
without thresholds	984	1352	1659	1129	1001	
including thresholds	1090	1494	1886	827	1067	

Tab. 4: Comparison of the originally reported gluino mass and the gluino mass including threshold corrections for previously published E_6SSM benchmarks, where we have chosen $\mu' = m_{H'} = m_{\bar{H}'} = 10$ TeV for all points except those marked [a] where we used $\mu' = m_{H'} = m_{\bar{H}'} = 100$ TeV to evade tachyonic problems with convergence and [b] where they were increased to 10^4 TeV.

is shown in Tab. 4 for $\mu' = m_{H'} = m_{\bar{H}'} = 10$ TeV, unless marked with [a] or [b] where the survival Higgs masses were varied until a self consistent solution could be found.

But while the survival Higgs masses can have important effects, all light benchmarks are left with a gluino mass substantially below the limit. Therefore we can confirm that all of these points have been excluded by the LHC even when threshold effects are taken account of and the survival Higgs masses are varied without regard to maintaining gauge coupling unification.

The situation is more optimistic for the new heavy benchmarks proposed in [10]. These benchmarks were chosen to satisfy the latest LHC limits and also have the right relic density. For the benchmarks HBM1–HBM3 there are significant changes to the gluino mass as shown in the third column of Tab. 4 pushing them further away from current constraints. However beyond this all qualitative features remain unchanged with the Higgs mass staying in the Higgs signal range, though it is modified to 125 GeV for HBM1 and HBM3. The light inert Higgsinos, fixed to be light to achieve the correct relic abundance density, remain light and can be tuned carefully to match the relic abundance density measurement exactly without perturbing the rest of the spectrum. HBM2 and HBM3 also have light exotic quarks and these also stay light, with their masses reduced by approximately 4 % and 6 % respectively. Therefore the essential features of these benchmarks are not changed

by the inclusion of threshold effects.

However for HBM4 and HBM5 the situation is more dramatic. These points have a very large singlet VEV, 50 TeV and 100 TeV respectively and in such cases while light gauginos can always be obtained, this is only achievable for a very narrow range of the input exotic Yukawa couplings. Consequentially when one varies these Yukawa couplings the masses can change a lot and the modification in these values (at low energies) from threshold corrections can result in very large changes to the soft masses. For HBM4 although a gluino mass of the same order is maintained the sign of $M_{1/2}$ is actually changed, while for HBM5 a positive $M_{1/2}$ is obtained but the stability of the result is not clear as scale variations lead to huge changes in the mass.

However these large changes in the physical spectrum are really an artifact of the choices for input/output parameters. One can instead try to match the values of m_0, $M_{1/2}$ and then observe changes in the exotic Yukawa couplings. This would typically lead to a similar spectrum, though λ_3 affects the light Higgs mass and therefore the light Higgs mass is shifted.

6 Summary and conclusions

In this paper we have improved the prediction of low-scale quantities from high-scale parameters in the Exceptional Supersymmetric Standard Model (E_6SSM). Full sparticle threshold corrections to the gauge couplings have been calculated by matching the E_6SSM to the SM. Similarly, the low-scale $\overline{\text{DR}}$ E_6SSM Yukawa couplings have been calculated at the loop level directly from mass measurements of the SM fermions and m_W. Full expressions for these corrections are provided, and we have implemented them into an improved spectrum generator for the constrained E_6SSM.

Using the spectrum generator, we have studied the impact of these corrections in detail. Both for the test point PP1 and in a parameter scan we found a dramatic reduction in the scale dependency of many masses, in particular of the gluino mass which is important for setting limits on the model from collider constraints. Also charginos, neutralinos, squarks and exotics receive large corrections. Even the smaller threshold effects for the light Higgs boson mass have a big impact on the allowed regions of parameter space due to our knowledge of the allowed values of the light Higgs mass, given recent LHC results on Higgs searches and the discovery of a new particle.

The new spectrum generator with the implemented corrections allows us to draw

firmer conclusions about the allowed parameter space of the model. In line with previous results, we found a substantial region of parameter space where the mass of lightest Higgs is compatible with the new boson discovered at the LHC and the limits from collider searches for squark, gluinos and Z' bosons, are all satisfied. However the threshold corrections imply a significant change in the high-scale parameters where this is achieved and can alter the way these constraints combine.

An interesting consequence of the threshold corrections is a dependency of the mass spectrum on the survival Higgs fields, which are included in the model to assist gauge coupling unification. In previous studies these states simply decoupled from the rest of the spectrum. With the full sparticle threshold corrections included, we found that in most of the spectrum the dependency of the spectrum is rather weak. However if the dependence on the unknown survival Higgs masses is viewed as a theoretical uncertainty, this uncertainty is larger than that from the remaining scale variation, though much smaller than the uncertainty of earlier studies neglecting threshold corrections.

If the survival Higgs bosons are taken seriously as physical fields, the threshold corrections allow to fix their masses by the requirement of gauge coupling unification. Indeed we found that the survival Higgs masses can always be chosen such that gauge coupling unification is valid, up to hypothetical GUT threshold corrections, with required survival Higgs masses in the multi-TeV region.

Finally we looked at how the threshold corrections affect benchmark points that have previously appeared in the literature. Many benchmarks proposed in earlier papers appeared to be ruled out by gluino searches. We confirmed all of these to be ruled out once the threshold corrections are included. The benchmarks proposed more recently to be consistent with experiment receive significant corrections. Nonetheless these benchmarks are still experimentally viable after including the threshold corrections. For two benchmarks, HBM4 and HBM5, the stability of the predictions is poor due to fine tuning of input parameters required to get the very hierarchical spectrum these benchmarks illustrate.

In conclusion, our study shows that it is possible and valuable to take into account higher-order corrections to the high-scale–low-scale connection even in complicated, non-minimal supersymmetric models such as the E_6SSM. The qualitative features of the CE_6SSM itself have not been changed by the threshold corrections. Still, the model is theoretically attractive, predictive and viable. As more LHC data comes in, distinguishing between different supersymmetric models and hypotheses of GUT-scale physics becomes more relevant, and precise spectrum generators like the one

presented here will be helpful.

Acknowledgements

The work of PA is supported by the ARC Centre of Excellence for Particle Physics at the Terascale, the work of AV is funded by the DFG Graduate College 1504, and we acknowledge financial support by the German Ministry for Science and Education. PA would like to thank S. F. King, A. Merle, D. J. Miller, M. Schönherr and Patrik Svantesson for helpful comments and discussions regarding this work.

A E$_6$SSM covariant derivative and GUT relations

The E_6 covariant derivative reads

$$D_\mu = \partial_\mu + \mathrm{i}g_0\tilde{A}^{\bar{a}}_\mu \tilde{T}^{\bar{a}} \qquad (\bar{a} = 1, \ldots, 78), \tag{A.1}$$

with a single gauge coupling g_0, where $\tilde{T}^{\bar{a}}$ are the generators and $\tilde{A}^{\bar{a}}_\mu$ are gauge fields in the adjoint representation (**78**) of the E_6. This covariant derivative can be decomposed in terms of the $SU(3)_{\rm c}$, $SU(2)_{\rm L}$, $U(1)_Y$ and $U(1)_N$ sub-groups

$$D_\mu = \partial_\mu + \mathrm{i}g_3 T^a G^a_\mu + \mathrm{i}g_2 \frac{\vec{\tau}}{2}\cdot\vec{W}_\mu + \mathrm{i}g_Y \frac{Y}{2} B_\mu + \mathrm{i}g_N \frac{N}{2} Z'_\mu + \cdots \tag{A.2}$$

All generators in (A.2) are normalized such that the quantum numbers are the same as in Tab. 1. This, together with the condition $\mathrm{Tr}\,\tilde{T}^a\tilde{T}^a = \delta^{ab}/2$, yields a GUT relation between the couplings

$$g_3 = g_2 = g_1 = g'_1 =: g_0, \tag{A.3}$$

where

$$g_1 := \sqrt{\frac{5}{3}}\, g_Y, \qquad g'_1 := \sqrt{40}\, g_N. \tag{A.4}$$

At the electroweak scale the generator Q of the unbroken $U(1)_{\rm em}$ is then given by

$$Q = \frac{\tau_3}{2} + \frac{Y}{2}. \tag{A.5}$$

B E$_6$SSM mass eigenstates

B.1 Higgs sector

We write the Higgs bosons in the E$_6$SSM as

$$H_{pi} = \begin{pmatrix} H^1_{pi} \\ H^2_{pi} \end{pmatrix}, \qquad S_i, \tag{B.1}$$

where $i = 1, 2, 3$ is the generation index and $p = 1, 2$ denotes the down ($p = 1$) and up ($p = 2$) Higgs bosons. When the $SU(2)_L \times U(1)_Y \times U(1)_N$ is broken to $U(1)_{\rm em.}$ the third generation Higgs bosons get a vacuum expectation value

$$H_{13} = \begin{pmatrix} H^0_{13} \\ H^-_{13} \end{pmatrix} \to \begin{pmatrix} \frac{v_1}{\sqrt{2}} + \Re\mathrm{e}\, H^0_{13} + i\,\Im\mathrm{m}\, H^0_{13} \\ H^-_{13} \end{pmatrix}, \tag{B.2}$$

$$H_{23} = \begin{pmatrix} H_{23}^+ \\ H_{23}^0 \end{pmatrix} \to \begin{pmatrix} H_{23}^+ \\ \frac{v_2}{\sqrt{2}} + \Re\mathrm{e}\, H_{23}^0 + i\, \Im\mathrm{m}\, H_{23}^0 \end{pmatrix}, \tag{B.3}$$

$$S_3 \to \frac{s}{\sqrt{2}} + \Re\mathrm{e}\, S_3 + i\, \Im\mathrm{m}\, S_3. \tag{B.4}$$

Furthermore we define

$$\tan\beta := \frac{v_2}{v_1}, \qquad \tan\phi := \frac{v}{2s}\sin 2\beta, \qquad \mu_{\mathrm{eff},i} := \frac{\lambda_i s}{\sqrt{2}}. \tag{B.5}$$

From the real parts of H_{13}^0, H_{23}^0 and S_3 we construct three CP even Higgs bosons. The diagonalization of the CP even mass matrix is done in two steps. At first we transform $\Re\mathrm{e}\, H_{13}^0$, $\Re\mathrm{e}\, H_{23}^0$ and $\Re\mathrm{e}\, S_3$ into intermediate states $(\mathsf{h}_1, \mathsf{h}_2, \mathsf{h}_3)$ via

$$\begin{pmatrix} \Re\mathrm{e}\, H_{13}^0 \\ \Re\mathrm{e}\, H_{23}^0 \\ \Re\mathrm{e}\, S_3 \end{pmatrix} = U_{\mathrm{MSSM}} \frac{1}{\sqrt{2}} \begin{pmatrix} \mathsf{h}_1 \\ \mathsf{h}_2 \\ \mathsf{h}_3 \end{pmatrix} + \frac{1}{\sqrt{2}} \begin{pmatrix} v_1 \\ v_2 \\ s \end{pmatrix}, \tag{B.6}$$

where the mixing matrix U_{MSSM} has the form

$$U_{\mathrm{MSSM}} = \begin{pmatrix} \cos\beta & -\sin\beta & 0 \\ \sin\beta & \cos\beta & 0 \\ 0 & 0 & 1 \end{pmatrix}. \tag{B.7}$$

In the basis of $\mathsf{h} = (\mathsf{h}_1, \mathsf{h}_2, \mathsf{h}_3)^T$ the Lagrangian for the CP even Higgs masses reads

$$\mathcal{L}_{\mathrm{even}} = -\frac{1}{2}\mathsf{h}^T M_{\mathrm{MSSM}} \mathsf{h}, \tag{B.8}$$

where the matrix M_{MSSM} is non-diagonal in general. Note, that the above transformation is analogous to the MSSM, where the mixing angle in U_{MSSM} is β. In a second step we diagonalize the mass matrix M_{MSSM} by the unitary matrix U_{E_6}. The resulting CP even Higgs mass eigenstates are labeled $h = (h_1, h_2, h_3)^T$. The diagonalization transformation reads

$$h = U_{E_6}\mathsf{h}, \qquad\qquad M_{E_6} = U_{E_6}^* M_{\mathrm{MSSM}} U_{E_6}^\dagger, \tag{B.9}$$

where M_{E_6} is diagonal. From the gauge eigenstates $\mathsf{A} = (\Im\mathrm{m}\, H_{13}^0, \Im\mathrm{m}\, H_{23}^0, \Im\mathrm{m}\, S_3)^T$ we construct three CP odd Higgs boson mass eigenstates $A = (A_1, A_2, A_3)^T \equiv (G^0, G', A^0)^T$ via

$$\frac{1}{\sqrt{2}} A := U_A \mathsf{A}, \qquad\qquad M_A = U_A^* M U_A^\dagger, \tag{B.10}$$

where M_A is diagonal. The mixing matrix U_A is parametrized as

$$U_A = \begin{pmatrix} \cos\beta & -\sin\beta & 0 \\ -\sin\beta\sin\phi & -\cos\beta\sin\phi & \cos\phi \\ \sin\beta\cos\phi & \cos\beta\cos\phi & \sin\phi \end{pmatrix}. \tag{B.11}$$

The charged Higgs and goldstone bosons $(H_i^\pm) = (G^\pm \; H^\pm)^T$ are constructed from the gauge eigenstates $H_{i3}^\pm$ via

$$H_i^\pm = U_{ij}^\pm H_{j3}^\pm \quad (i,j=1,2), \qquad \text{where} \qquad U^\pm = \begin{pmatrix} \cos\beta & -\sin\beta \\ \sin\beta & \cos\beta \end{pmatrix}. \tag{B.12}$$

B.2 Inert Higgs sector

The first two generations ($i = 1,2;\ p = 1,2$) Higgs doublets in Eq. (B.1) are called inert Higgs bosons. For each generation $i = 1,2$ we mix the fields H_{1i}^0, H_{2i}^{0*} to mass eigenstates h_{ik}^0 with an unitary matrix U_{inert}^{0i} via

$$h_{ik}^0 = (U_{\text{inert}}^{0i})_{kl} \begin{pmatrix} H_{1i}^0 \\ H_{2i}^{0*} \end{pmatrix}_l, \qquad U_{\text{inert}}^{0i} = \begin{pmatrix} \cos\theta_i^0 & \sin\theta_i^0 \\ -\sin\theta_i^0 & \cos\theta_i^0 \end{pmatrix}. \tag{B.13}$$

Here $k,l = 1,2$ enumerates the mass eigenstates and we neglect inter-generation mixing. Furthermore for each generation $i = 1,2$ we mix the fields H_{1i}^-, H_{2i}^{+*} to mass eigenstates h_{ik}^- with an unitary matrix $U_{\text{inert}}^{\pm i}$ via

$$h_{ik}^- = (U_{\text{inert}}^{\pm i})_{kl} \begin{pmatrix} H_{1i}^- \\ H_{2i}^{+*} \end{pmatrix}_l, \qquad U_{\text{inert}}^{\pm i} = \begin{pmatrix} \cos\theta_i^\pm & \sin\theta_i^\pm \\ -\sin\theta_i^\pm & \cos\theta_i^\pm \end{pmatrix}. \tag{B.14}$$

Here $k,l = 1,2$ enumerates the mass eigenstates and we neglect inter-generation mixing. Furthermore for each generation $i = 1,2$ we mix the fields $\tilde{H}_{1iL}^0$, $\tilde{H}_{2iL}^0$ to mass eigenstates ψ_{li}^0 with an unitary matrix Z via

$$\psi_{li}^0 = Z_{ln} \begin{pmatrix} \tilde{H}_{1iL}^0 \\ \tilde{H}_{2iL}^0 \end{pmatrix}_n, \qquad Z = \frac{1}{\sqrt{2}} \begin{pmatrix} 1 & 1 \\ -1 & 1 \end{pmatrix}. \tag{B.15}$$

The Majorana mass eigenstates are then defined as

$$\tilde{h}_{li}^0 = \begin{pmatrix} \psi_{li}^0 \\ \overline{\psi_{li}^0}^T \end{pmatrix}. \tag{B.16}$$

For each generation $i = 1,2$ we combine the fields $\tilde{H}_{1iL}^-$, $\overline{\tilde{H}_{2iL}^+}^T$ to mass eigenstates $\tilde{h}_i^-$ via

$$\tilde{h}_i^- = \begin{pmatrix} \tilde{H}_{1iL}^- \\ \overline{\tilde{H}_{2iL}^+}^T \end{pmatrix}. \tag{B.17}$$

B.3 Survival Higgs sector

We mix the neutral survival Higgs bosons H'^0, $\bar{H}'^{0*}$ to mass eigenstates h'^0_k with an unitary matrix $U^0_{\rm surv}$ via

$$h'^0_k = (U^0_{\rm surv})_{kl} \begin{pmatrix} H'^0 \\ \bar{H}'^{0*} \end{pmatrix}_l, \qquad U^0_{\rm surv} = \begin{pmatrix} \cos\theta'^0 & \sin\theta'^0 \\ -\sin\theta'^0 & \cos\theta'^0 \end{pmatrix}. \tag{B.18}$$

We mix the charged survival Higgs bosons H'^-, $\bar{H}'^{+*}$ to mass eigenstates h'^-_k with an unitary matrix $U^\pm_{\rm surv}$ via

$$h'^-_k = (U^\pm_{\rm surv})_{kl} \begin{pmatrix} H'^- \\ \bar{H}'^{+*} \end{pmatrix}_l, \qquad U^\pm_{\rm surv} = \begin{pmatrix} \cos\theta'^\pm & \sin\theta'^\pm \\ -\sin\theta'^\pm & \cos\theta'^\pm \end{pmatrix}. \tag{B.19}$$

The survival higgsinos obey the same mixing as the neutral and charged inert higgsinos in Sec. B.2. We write the mass eigenstates as $\tilde{h}'^\pm$ and $\tilde{h}'^0_i$ $(i = 1, 2)$.

C E_6SSM self-energies

C.1 W boson

The $W^\pm$ boson 1PI correlation function is decomposed into a transverse and longitudinal part as follows

$$\Gamma_{W^+_\mu W^-_\nu}(p) = -g^{\mu\nu}(p^2 - m_W^2) - \left(g^{\mu\nu} - \frac{p^\mu p^\nu}{p^2}\right)\Pi_{WW,T}(p^2) - \frac{p^\mu p^\nu}{p^2}\Pi_{WW,L}(p^2), \tag{C.1}$$

where the transverse part is in the E_6SSM given by

$$\begin{aligned}
\frac{(4\pi)^2}{g_2^2}\Pi^{\rm E_6SSM}_{WW,T}(p^2) = {} & \frac{1}{4}\sum_{i=1}^{3}\sum_{k=1}^{2}\left\{\left(U^{A*}_{ik}\right)^2 A_0(m_{A_i}) + \left(U^{E_6*}_{ik}\right)^2 A_0(m_{h_i})\right\} \\
& + \frac{1}{2}A_0(m_{H^\pm}) + \frac{1}{2}A_0(m_{G^\pm}) + m_W^2\sum_{i=1}^{3}\left(U^{E_6*}_{i1}\right)^2 B_0(p^2, m_{h_i}, m_W) \\
& - \sum_{i=1}^{3}\sum_{j=1}^{2}\left|U^A_{i1}U^\pm_{j1} + U^A_{i2}U^\pm_{j2}\right|^2 B_{22}(p^2, m_{A_i}, m_{H^\pm_j}) \\
& - \sum_{i=1}^{3}\sum_{j=1}^{2}\left|\sum_{k=1}^{3} U^{E_6}_{ik}\left(U^{\rm MSSM}_{1k}U^\pm_{j1} - U^{\rm MSSM}_{2k}U^\pm_{j2}\right)\right|^2 B_{22}(p^2, m_{A_i}, m_{H^\pm_j}) \\
& + \sum_{i,l=1}^{2}\left\{\frac{1}{2}\left(|Z_{l1}|^2 + |Z_{l2}|^2\right)H(p^2, m_{\tilde{h}^+_i}, m_{\tilde{h}^0_{li}})\right.
\end{aligned}$$

$$
\begin{aligned}
&\quad - 2Z_{l1}Z_{l2}m_{\tilde{h}_i^+}m_{\tilde{h}_{li}^0}B_0(p^2,m_{\tilde{h}_i^+},m_{\tilde{h}_{li}^0})\Big\}\\
&- 2\sum_{i=1}^{2}\Big\{\cos^2(\theta_i^0+\theta_i^\pm)\left(\widetilde{B}_{22}(p^2,m_{h_{i1}^\pm},m_{h_{i1}^0})+\widetilde{B}_{22}(p^2,m_{h_{i2}^\pm},m_{h_{i2}^0})\right)\\
&\qquad + \sin^2(\theta_i^0+\theta_i^\pm)\left(\widetilde{B}_{22}(p^2,m_{h_{i1}^\pm},m_{h_{i2}^0})+\widetilde{B}_{22}(p^2,m_{h_{i2}^\pm},m_{h_{i1}^0})\right)\Big\}\\
&+\sum_{l=1}^{2}\Big\{\frac{1}{2}\left(|Z'_{l1}|^2+|Z'_{l2}|^2\right)H(p^2,m_{\tilde{h}'^+},m_{\tilde{h}_l'^0})\\
&\quad - 2Z'_{l1}Z'_{l2}m_{\tilde{h}'^+}m_{\tilde{h}_l'^0}B_0(p^2,m_{\tilde{h}'^+},m_{\tilde{h}_l'^0})\Big\}\\
&- 2\sum_{i=1}^{2}\Big\{\cos^2(\theta'^0+\theta'^\pm)\left(\widetilde{B}_{22}(p^2,m_{h'^\pm_1},m_{h'^0_1})+\widetilde{B}_{22}(p^2,m_{h'^\pm_2},m_{h'^0_2})\right)\\
&\qquad + \sin^2(\theta'^0+\theta'^\pm)\left(\widetilde{B}_{22}(p^2,m_{h'^\pm_1},m_{h'^0_2})+\widetilde{B}_{22}(p^2,m_{h'^\pm_2},m_{h'^0_1})\right)\Big\}\\
&+4m_W^2\frac{g_N^2}{g_2^2}\Big\{\left(\frac{N_{H_{13}}}{2}+\frac{N_{H_{23}}}{2}\right)^2\sin^2\beta\cos^2\beta B_0(p^2,m_{H^\pm},m_{Z'})\\
&\qquad +\left(\frac{N_{H_{23}}}{2}\sin^2\beta-\frac{N_{H_{13}}}{2}\cos^2\beta\right)^2 B_0(p^2,m_{G^\pm},m_{Z'})\Big\}\\
&-s_W^2\left(8\widetilde{B}_{22}(p^2,m_W,0)+4p^2B_0(p^2,m_W,0)\right)\\
&-\left\{(4p^2+m_Z^2+m_W^2)c_W^2-m_Z^2s_W^4\right\}B_0(p^2,m_Z,m_W)\\
&-8c_W^2\widetilde{B}_{22}(p^2,m_Z,m_W)\\
&+\sum_{f_u/f_d}\left\{\frac{1}{2}N_c^f H(p^2,m_u,m_d)-\sum_{i,j=1}^{2}2N_c^f w_{fij}^2\widetilde{B}_{22}(p^2,m_{\tilde{u}_i},m_{\tilde{d}_j})\right\}\\
&+\frac{1}{g_2^2}\sum_{i=1}^{6}\sum_{j=1}^{2}\left\{f_{ijW}H(p^2,m_{\tilde{\chi}_i^0},m_{\tilde{\chi}_j^+})+2g_{ijW}m_{\tilde{\chi}_i^0}m_{\tilde{\chi}_j^+}B_0(p^2,m_{\tilde{\chi}_i^0},m_{\tilde{\chi}_j^+})\right\}
\end{aligned}
\tag{C.2}
$$

Analogous to [59] the summation $\sum_{f_u/f_d}$ is over quark and lepton doublets and

$$
(w_{fij})=\begin{pmatrix}c_uc_d & c_us_d\\ s_uc_d & s_us_d\end{pmatrix}. \tag{C.3}
$$

The neutralino–chargino–W-boson couplings are given by

$$
f_{ijW}=|a_{\tilde{\chi}_i^0\tilde{\chi}_j^+W}|^2+|b_{\tilde{\chi}_i^0\tilde{\chi}_j^+W}|^2,\qquad g_{ijW}=2\,\Re\mathrm{e}\left(b^*_{\tilde{\chi}_i^0\tilde{\chi}_j^+W}a_{\tilde{\chi}_i^0\tilde{\chi}_j^+W}\right), \tag{C.4}
$$

where the Feynman rule for the neutralino–chargino–W_μ vertex is written as $-i\gamma_\mu(a\mathcal{P}_L + b\mathcal{P}_R)$. The nonzero couplings in the E$_6$SSM are the same as in the MSSM

$$a_{\tilde{\psi}_2^0\tilde{\psi}_1^+W} = b_{\tilde{\psi}_2^0\tilde{\psi}_1^+W} = -g_2, \qquad a_{\tilde{\psi}_4^0\tilde{\psi}_2^+W} = -b_{\tilde{\psi}_3^0\tilde{\psi}_2^+W} = \frac{g_2}{\sqrt{2}}. \tag{C.5}$$

The couplings to mass eigenstates for an incoming neutralino $\tilde{\chi}_i^0$ are

$$a_{\tilde{\chi}_i^0\tilde{\chi}_j^+W} = N_{ik}^* V_{jl} a_{\tilde{\psi}_k^0\tilde{\psi}_l^+W}, \qquad b_{\tilde{\chi}_i^0\tilde{\chi}_j^+W} = N_{ik} U_{jl}^* b_{\tilde{\psi}_k^0\tilde{\psi}_l^+W}, \tag{C.6}$$

while for an incoming chargino $\tilde{\chi}_j^+$ the couplings read

$$a_{\tilde{\chi}_i^0\tilde{\chi}_j^+W} = N_{ik} V_{jl}^* a_{\tilde{\psi}_k^0\tilde{\psi}_l^+W}, \qquad b_{\tilde{\chi}_i^0\tilde{\chi}_j^+W} = N_{ik}^* U_{jl} b_{\tilde{\psi}_k^0\tilde{\psi}_l^+W}. \tag{C.7}$$

C.2 Fermions

We decompose the fermion 1PI correlation function as

$$\Gamma_{f\bar{f}}(p) = \not{p}\left(P_L\Gamma_{f\bar{f}}^L(p^2) + P_R\Gamma_{f\bar{f}}^R(p^2)\right) + P_L\Gamma_{f\bar{f}}^l(p^2) + P_R\Gamma_{f\bar{f}}^r(p^2) \tag{C.8}$$

and then define the fermion self-energy to be

$$\Sigma_f(p^2) := \frac{1}{2}\left\{m_f\left[\Gamma_{f\bar{f}}^L(p^2) + \Gamma_{f\bar{f}}^R(p^2)\right] + \Gamma_{f\bar{f}}^l(p^2) + \Gamma_{f\bar{f}}^r(p^2)\right\}. \tag{C.9}$$

In the E$_6$SSM it is given by

$$\begin{aligned}
(4\pi)^2\frac{\Sigma_t(p^2)}{m_t} = \frac{4g_3^2}{3}\Bigg\{ & B_1(p^2, m_{\tilde{g}}, m_{\tilde{t}_1}) + B_1(p^2, m_{\tilde{g}}, m_{\tilde{t}_2}) - \left(5 + 3\ln\frac{\mu^2}{m_t^2}\right) \\
& - \sin(2\theta_t)\frac{m_{\tilde{g}}}{m_t}\left(B_0(p^2, m_{\tilde{g}}, m_{\tilde{t}_1}) - B_0(p^2, m_{\tilde{g}}, m_{\tilde{t}_2})\right)\Bigg\} \\
& + \frac{y_t^2}{2}\sum_{i=1}^{3}\Big\{\underline{A}_{ti}^2\left[B_1(p^2, m_t, m_{h_i}) + B_0(p^2, m_t, m_{h_i})\right] \\
& \qquad + \underline{B}_{ti}^2\left[B_1(p^2, m_t, m_{A_i}) - B_0(p^2, m_t, m_{A_i})\right]\Big\} \\
& + \frac{1}{2}\Big[(y_b^2 s_\beta^2 + y_t^2 c_\beta^2)B_1(p^2, m_b, m_{H^+}) + (g_2^2 + y_b^2 c_\beta^2 + y_t^2 s_\beta^2)B_1(p^2, m_b, m_W)\Big] \\
& + y_b^2 c_\beta^2\Big[B_0(p^2, m_b, m_{H^+}) - B_0(p^2, m_b, m_W)\Big] - (ee_t)^2\left(5 + 3\ln\frac{\mu^2}{m_t^2}\right) \\
& + \frac{g_2^2}{c_W^2}\Big[\left(g_{t_L}^2 + g_{t_R}^2\right)B_1(p^2, m_t, m_Z) + 4g_{t_L}g_{t_R}B_0(p^2, m_t, m_Z)\Big] \\
& + \frac{1}{2}\sum_{i=1}^{6}\sum_{j=1}^{2}\Big[f_{it\tilde{t}_j}B_1(p^2, m_{\tilde{\chi}_i^0}, m_{\tilde{t}_j}) + g_{it\tilde{t}_j}\frac{m_{\tilde{\chi}_i^0}}{m_t}B_0(p^2, m_{\tilde{\chi}_i^0}, m_{\tilde{t}_j})\Big]
\end{aligned}$$

$$+\frac{1}{2}\sum_{i,j=1}^{2}\left[f_{it\tilde{b}_j}B_1(p^2,m_{\tilde{\chi}_i^+},m_{\tilde{b}_j})+g_{it\tilde{b}_j}\frac{m_{\tilde{\chi}_i^+}}{m_t}B_0(p^2,m_{\tilde{\chi}_i^+},m_{\tilde{b}_j})\right]$$
$$+g_N^2\left[\left(\left(\frac{N_{t_L}}{2}\right)^2+\left(\frac{N_{t_R}}{2}\right)^2\right)B_1(p^2,m_t,m_{Z'})+N_{t_L}N_{t_R}B_0(p^2,m_t,m_{Z'})\right] \tag{C.10}$$

The matrix elements $\underline{A}_{fi}$ and $\underline{B}_{fi}$ are defined as

$$\underline{A}_{fi}=\begin{cases}(U_{\rm MSSM})_{2k}(U_{E_6})^*_{ik} & \text{if } f \text{ is up-type,}\\ (U_{\rm MSSM})_{1k}(U_{E_6})^*_{ik} & \text{if } f \text{ is down-type,}\end{cases} \tag{C.11}$$

$$\underline{B}_{fi}=\begin{cases}(U_A)^*_{i2} & \text{if } f \text{ is up-type,}\\ (U_A)^*_{i1} & \text{if } f \text{ is down-type.}\end{cases} \tag{C.12}$$

In analogy to [59] the Feynman rules for the $\tilde{\chi}_i f\tilde{f}_j$ couplings are written as $-i(a\mathcal{P}_L+b\mathcal{P}_R)$ and we have defined

$$f_{if\tilde{f}_j}=|a_{\tilde{\chi}_i f\tilde{f}_j}|^2+|b_{\tilde{\chi}_i f\tilde{f}_j}|^2,\qquad g_{if\tilde{f}_j}=2\,\Re\mathrm{e}(b^*_{\tilde{\chi}_i f\tilde{f}_j}a_{\tilde{\chi}_i f\tilde{f}_j}). \tag{C.13}$$

In the gauge eigenstate basis $\tilde{\psi}^0,\tilde{\psi}^+$ one has

$$a_{\tilde{\psi}_1^0 f\tilde{f}_R}=\frac{g_Y}{\sqrt{2}}Y_{f_R},\qquad b_{\tilde{\psi}_1^0 f\tilde{f}_L}=\frac{g_Y}{\sqrt{2}}Y_{f_L} \tag{C.14}$$
$$b_{\tilde{\psi}_2^0 f\tilde{f}_L}=\sqrt{2}g_2\tau_3^{f_L},\qquad a_{\tilde{\psi}_1^+ d\tilde{u}_L}=b_{\tilde{\psi}_1^+ u\tilde{d}_L}=g_2, \tag{C.15}$$
$$a_{\tilde{\psi}_3^0 d\tilde{d}_L}=b_{\tilde{\psi}_3^0 d\tilde{d}_R}=-b_{\tilde{\psi}_2^+ d\tilde{u}_L}=-b_{\tilde{\psi}_2^+ u\tilde{d}_R}=y_d, \tag{C.16}$$
$$a_{\tilde{\psi}_4^0 u\tilde{u}_L}=b_{\tilde{\psi}_4^0 u\tilde{u}_R}=-a_{\tilde{\psi}_2^+ u\tilde{d}_L}=-a_{\tilde{\psi}_2^+ d\tilde{u}_R}=y_u, \tag{C.17}$$
$$a_{\tilde{\psi}_6^0 f\tilde{f}_R}=\frac{g_N}{\sqrt{2}}N_{f_R},\qquad b_{\tilde{\psi}_6^0 f\tilde{f}_L}=\frac{g_N}{\sqrt{2}}N_{f_L}, \tag{C.18}$$

where the quantum numbers $Y_f/2$, $N_f/2$ and τ_3^f are listed in the Tab. 1. The couplings to the mass eigenstates $\tilde{\chi}_i^0$ and $\tilde{\chi}_i^+$ are obtained by the rotations

$$a_{\tilde{\chi}_i^0 f\tilde{f}}=N^*_{ij}a_{\tilde{\psi}_j^0 f\tilde{f}},\qquad b_{\tilde{\chi}_i^0 f\tilde{f}}=N_{ij}b_{\tilde{\psi}_j^0 f\tilde{f}}, \tag{C.19}$$
$$a_{\tilde{\chi}_i^+ f\tilde{f}'}=V^*_{ij}a_{\tilde{\psi}_j^+ f\tilde{f}'},\qquad b_{\tilde{\chi}_i^+ f\tilde{f}'}=U_{ij}b_{\tilde{\psi}_j^+ f\tilde{f}'}. \tag{C.20}$$

To obtain the couplings to the sfermion mass eigenstates one rotates these couplings (both a- and b-type) by the sfermion mixing matrix,

$$\begin{pmatrix}a_{\tilde{\chi}f\tilde{f}'_1}\\ a_{\tilde{\chi}f\tilde{f}'_2}\end{pmatrix}=\begin{pmatrix}c_{f'} & s_{f'}\\ -s_{f'} & c_{f'}\end{pmatrix}\begin{pmatrix}a_{\tilde{\chi}f\tilde{f}'_L}\\ a_{\tilde{\chi}f\tilde{f}'_R}\end{pmatrix}. \tag{C.21}$$

The self-energies for the other fermions are obtained from Σ_t by the substitutions

$$\Sigma_\tau(p^2) = \Sigma_t(p^2)\big|_{t\to b, g_3=0}\,, \tag{C.22}$$

$$\Sigma_b(p^2) = \Sigma_t(p^2)\big|_{t\to b, c_\beta\leftrightarrow s_\beta}\,. \tag{C.23}$$

In Eqs. (C.2) and (C.10) we use the loop functions as defined in [59].

D E$_6$SSM counterterms

If not otherwise stated we renormalize the $W^\pm$ boson and the SM fermions in the on-shell scheme. The corresponding on-shell and $\overline{\rm DR}$ counterterms are

$$\delta m_W^{2,\text{on-shell}} = \widetilde{\Re\text{e}}\,\Pi_{WW,T}(m_W^2), \qquad \delta m_W^{2,\overline{\rm DR}} = \widetilde{\Re\text{e}}\,\Pi_{WW,T}(m_W^2)\Big|_\Delta \tag{D.1}$$

$$\delta m_f^{\text{on-shell}} = \widetilde{\Re\text{e}}\,\Sigma_f(m_f^2), \qquad \delta m_f^{\overline{\rm DR}} = \widetilde{\Re\text{e}}\,\Sigma_f(m_f^2)\Big|_\Delta \tag{D.2}$$

where the self-energies $\Pi_{WW,T}$ and Σ_f are given in Eqs. (C.2), (C.10), (C.22) and (C.23). Using Eqs. (C.2) and (C.10) one can derive the following divergences for the δm_W and δm_f counterterms in the E$_6$SSM

$$\begin{aligned}\frac{\delta m_W}{m_W}\bigg|_\Delta = \frac{\Delta}{(4\pi)^2}\Bigg\{&\frac{11}{2}g_2^2 + \frac{1}{2}g_Y^2 + 2g_N^2\left[\left(\frac{N_{H_{13}}}{2}\right)^2\cos^2\beta + \left(\frac{N_{H_{23}}}{2}\right)^2\sin^2\beta\right]\\ &- \lambda_3^2 - 3y_t^2\sin^2\beta - 3y_b^2\cos^2\beta - y_\tau^2\cos^2\beta\Bigg\},\end{aligned} \tag{D.3}$$

$$\begin{aligned}\frac{\delta m_{f_u}}{m_{f_u}}\bigg|_\Delta = \frac{\Delta}{(4\pi)^2}\Bigg\{&-2g_3^2 C_2(r(f_u))_{SU(3)_c} - \frac{3}{4}g_2^2 - g_N^2\left[\left(\frac{N_{L,f_u}}{2}\right)^2 + \left(\frac{N_{R,f_u}}{2}\right)^2\right]\\ &-g_Y^2\left[\left(\frac{Y_{L,f_u}}{2}\right)^2 + \left(\frac{Y_{R,f_u}}{2}\right)^2\right] + \frac{3}{2}y_{f_u}^2 + \frac{1}{2}y_{f_d}^2\Bigg\},\end{aligned} \tag{D.4}$$

$$\begin{aligned}\frac{\delta m_{f_d}}{m_{f_d}}\bigg|_\Delta = \frac{\Delta}{(4\pi)^2}\Bigg\{&-2g_3^2 C_2(r(f_d))_{SU(3)_c} - \frac{3}{4}g_2^2 - g_N^2\left[\left(\frac{N_{L,f_d}}{2}\right)^2 + \left(\frac{N_{R,f_d}}{2}\right)^2\right]\\ &-g_Y^2\left[\left(\frac{Y_{L,f_d}}{2}\right)^2 + \left(\frac{Y_{R,f_d}}{2}\right)^2\right] + \frac{3}{2}y_{f_d}^2 + \frac{1}{2}y_{f_u}^2\Bigg\}.\end{aligned} \tag{D.5}$$

Here $C_2(r)_{SU(N)}$ is a representation invariant of the representation r of $SU(N)$ and defined by

$$C_2(N)_{SU(N)} = \frac{N^2-1}{2N} \qquad \text{(fundamental representation } N\text{)}, \tag{D.6}$$

$$C_2(G)_{SU(N)} = N \qquad \text{(adjoint representation } G\text{)}. \tag{D.7}$$

Especially we have $C_2(r_{f_u})_{SU(3)_c} = C_2(r_{f_d})_{SU(3)_c} = 4/3$. Furthermore it follows from the one-loop β functions (D.9)–(D.12) that the divergences of δg_i in the SM and the E$_6$SSM are given by

$$\left.\frac{\delta g_i}{g_i}\right|_{\Delta} = \frac{\Delta}{(4\pi)^2}\frac{\beta_i}{2}g_i^2, \tag{D.8}$$

$$\beta_3^{\mathrm{E_6SSM}} = 0, \qquad \beta_3^{\mathrm{SM}} = -7, \tag{D.9}$$

$$\beta_2^{\mathrm{E_6SSM}} = 4, \qquad \beta_2^{\mathrm{SM}} = -\frac{19}{6}, \tag{D.10}$$

$$\beta_1^{\mathrm{E_6SSM}} = \frac{3}{5}\beta_Y^{\mathrm{E_6SSM}} = \frac{48}{5}, \qquad \beta_1^{\mathrm{SM}} = \frac{3}{5}\beta_Y^{\mathrm{SM}} = \frac{41}{10}, \tag{D.11}$$

$$\beta_1'^{\,\mathrm{E_6SSM}} = \frac{1}{40}\beta_N^{\mathrm{E_6SSM}} = \frac{47}{5}. \tag{D.12}$$

The divergence of $\delta\tan\beta$ in the E$_6$SSM is

$$\left.\frac{\delta\tan\beta}{\tan\beta}\right|_{\Delta} = \frac{\Delta}{(4\pi)^2}\frac{\beta_{\tan\beta}}{2}, \tag{D.13}$$

from which we obtain the one-loop RGE for $\tan\beta$,

$$\frac{\mathrm{d}\tan\beta}{\mathrm{d}t} = \frac{\tan\beta}{(4\pi)^2}\beta_{\tan\beta}, \tag{D.14}$$

$$\beta_{\tan\beta} = 2\left\{\frac{3}{2}y_b^2 + \frac{1}{2}y_\tau^2 - \frac{3}{2}y_t^2 - g_N^2\left[\left(\frac{N_{H_{13}}}{2}\right)^2 - \left(\frac{N_{H_{23}}}{2}\right)^2\right]\right\}, \tag{D.15}$$

needed so that we consistently input $\tan\beta$, defined at a fixed scale, when we vary the matching scale where the Yukawas are calculated.

References

[1] P. Athron, J. P. Hall, R. Howl, S. F. King, D. J. Miller, S. Moretti and R. Nevzorov, Nucl. Phys. Proc. Suppl. **200-202**, 120 (2010).

[2] S. F. King, S. Moretti, R. Nevzorov, Phys. Rev. D **73** (2006) 035009.

[3] S. F. King, S. Moretti, R. Nevzorov, Phys. Lett. B **634** (2006) 278.

[4] J. E. Kim and H. P. Nilles, Phys. Lett. B **138** (1984) 150.

[5] U. Ellwanger, C. Hugonie and A. M. Teixeira, Phys. Rept. **496**, 1 (2010) [arXiv:0910.1785 [hep-ph]], M. Maniatis, Int. J. Mod. Phys. A **25** (2010) 3505 [arXiv:0906.0777 [hep-ph]].

[6] P.Fayet, Nucl.Phys. B 90 (1975) 104; H.P.Nilles, M.Srednicki, D.Wyler, Phys.Lett.B 120 (1983) 346; J.M.Frere, D.R.T.Jones, S.Raby, Nucl.Phys.B 222 (1983) 11; J.P.Derendinger, C.A.Savoy, Nucl.Phys.B 237 (1984) 307. M.I.Vysotsky, K.A.Ter-Martirosian, Sov.Phys.JETP 63 (1986) 489; J.Ellis, J.F.Gunion, H.Haber, L.Roszkowski, F.Zwirner, Phys.Rev.D 39 (1989) 844.

[7] F. del Aguila, G. A. Blair, M. Daniel, G. G. Ross, Nucl. Phys. B **272** (1986) 413.

[8] P. Athron, S. F. King, D. J. Miller, S. Moretti and R. Nevzorov, Phys. Rev. D **80**, 035009 (2009) [arXiv:0904.2169 [hep-ph]].

[9] P. Athron, S. F. King, D. J. Miller, S. Moretti and R. Nevzorov, Phys. Lett. B **681**, 448 (2009) [arXiv:0901.1192 [hep-ph]].

[10] P. Athron, S. F. King, D. J. Miller, S. Moretti and R. Nevzorov, arXiv:1206.5028 [hep-ph].

[11] R. Howl and S. F. King, Phys. Lett. B **652**, 331 (2007) [arXiv:0705.0301 [hep-ph]].

[12] R. Howl and S. F. King, JHEP **0801**, 030 (2008) [arXiv:0708.1451 [hep-ph]].

[13] R. Howl and S. F. King, JHEP **0805**, 008 (2008) [arXiv:0802.1909 [hep-ph]].

[14] J. Erler, P. Langacker, S. Munir and E. Rojas, JHEP **0908**, 017 (2009) [arXiv:0906.2435 [hep-ph]].

[15] R. Howl and S. F. King, Phys. Lett. B **687**, 355 (2010) [arXiv:0908.2067 [hep-ph]].

[16] F. Braam, A. Knochel and J. Reuter, JHEP **1006**, 013 (2010) [arXiv:1001.4074 [hep-ph]].

[17] J. P. Hall, S. F. King, R. Nevzorov, S. Pakvasa and M. Sher, arXiv:1109.4972 [hep-ph].

[18] A. Belyaev, J. P. Hall, S. F. King and P. Svantesson, arXiv:1203.2495 [hep-ph].

[19] T. G. Rizzo, Phys. Rev. D **85**, 055010 (2012) [arXiv:1201.2898 [hep-ph]].

[20] R. Nevzorov, arXiv:1205.5967 [hep-ph].

[21] D. J. Miller, A. P. Morais and P. N. Pandita, arXiv:1208.5906 [hep-ph].

[22] W. Porod, Comput. Phys. Commun. **153**, 275 (2003) [arXiv:hep-ph/0301101].

[23] A. Djouadi, J. L. Kneur and G. Moultaka, Comput. Phys. Commun. **176**, 426 (2007) [arXiv:hep-ph/0211331].

[24] B. C. Allanach, Comput. Phys. Commun. **143**, 305 (2002) [arXiv:hep-ph/0104145].

[25] F. E. Paige, S. D. Protopopescu, H. Baer and X. Tata, arXiv:hep-ph/0312045.

[26] D. Chowdhury, R. Garani and S. KVempati, arXiv:1109.3551 [hep-ph].

[27] G. Belanger, S. Kraml and A. Pukhov, Phys. Rev. D **72**, 015003 (2005) [arXiv:hep-ph/0502079].

[28] G. Aad *et al.* [ATLAS Collaboration], arXiv:1207.7214 [hep-ex].

[29] S. Chatrchyan *et al.* [CMS Collaboration], [arXiv:1207.7235 [hep-ex]].

[30] S. F. King, S. Moretti and R. Nevzorov, Phys. Lett. B **650**, 57 (2007) [arXiv:hep-ph/0701064].

[31] P. Athron, S. F. King, R. Luo, D. J. Miller, S. Moretti and R. Nevzorov, AIP Conf. Proc. **1200**, 466 (2010) [arXiv:0909.4530 [hep-ph]].

[32] Y. Hosotani, Phys. Lett. B **126** (1983) 309.

[33] J.L. Hewett, T.G. Rizzo, Phys. Rept. **183** (1989) 193;

[34] P. Langacker, Rev. Mod. Phys. **81**, 1199 (2009)

[35] J. Rich, D. Lloyd Owen and M. Spiro, Phys. Rept. **151**, 239 (1987).

[36] P. F. Smith, Contemp. Phys. **29**, 159 (1988).

[37] T. K. Hemmick *et al.*, Phys. Rev. D **41**, 2074 (1990).

[38] B. A. Ovrut and H. J. Schnitzer, Nucl. Phys. B **184** (1981) 109.

[39] L. J. Hall, Nucl. Phys. B **178** (1981) 75.

[40] S. P. Martin and M. T. Vaughn, Phys. Lett. B **318** (1993) 331 [arXiv:hep-ph/9308222].

[41] K. Nakamura *et al.* [Particle Data Group], J. Phys. G **37** (2010) 075021.

[42] H. Baer, J. Ferrandis, K. Melnikov and X. Tata, Phys. Rev. D **66** (2002) 074007 [hep-ph/0207126].

[43] The ATLAS Collaboration, ATLAS-CONF-2012-033.

[44] The ATLAS Collaboration, ATLAS-CONF-2012-037.

[45] The ATLAS Collaboration, ATLAS-CONF-2012-041.

[46] C. Rogan, arXiv:1006.2727 [hep-ph].

[47] The CMS Collaboration, CMS PAS SUS-12-005 (2012).

[48] The CMS Collaboration, CMS PAS SUS-12-002 (2012).

[49] The ATLAS Collaboration, ATLAS-CONF-2012-103. The ATLAS Collaboration, ATLAS-CONF-2012-104. The ATLAS Collaboration, ATLAS-CONF-2012-105. The ATLAS Collaboration, ATLAS-CONF-2012-109.

[50] P. Athron, S. F. King, D. J. Miller, S. Moretti and R. Nevzorov, Phys. Rev. D **84**, 055006 (2011) [arXiv:1102.4363 [hep-ph]].

[51] G. Aad *et al.* [ATLAS Collaboration], Phys. Lett. B **710** (2012) 49 [arXiv:1202.1408 [hep-ex]].

[52] S. Chatrchyan *et al.* [CMS Collaboration], Phys. Lett. B **710** (2012) 26 arXiv:1202.1488 [hep-ex].

[53] S. Chatrchyan *et al.* [CMS Collaboration], arXiv:1206.1849 [hep-ex].

[54] J. P. Hall and S. F. King, JHEP **0908**, 088 (2009) [arXiv:0905.2696 [hep-ph]].

[55] J. P. Hall, S. F. King, R. Nevzorov, S. Pakvasa, M. Sher, R. Nevzorov, S. Pakvasa and M. Sher, Phys. Rev. D **83**, 075013 (2011) [arXiv:1012.5114 [hep-ph]].

[56] S. F. King and A. Merle, arXiv:1205.0551 [hep-ph].

[57] J. P. Hall and S. F. King, JHEP **1106**, 006 (2011) [arXiv:1104.2259 [hep-ph]].

[58] M. S. Carena, M. Olechowski, S. Pokorski and C. E. M. Wagner, Nucl. Phys. B **426**, 269 (1994) [hep-ph/9402253].

[59] D. M. Pierce, J. A. Bagger, K. T. Matchev and R. -j. Zhang, Nucl. Phys. B **491** (1997) 3 [hep-ph/9606211].